Theses and Dissertations                    1. Thesis and Dissertation Collection, all items

2010-03

# Performance characterization of swept ramp obstacle fields in pulse detonation applications

## Dvorak, William T.

Monterey, California. Naval Postgraduate School

http://hdl.handle.net/10945/10544

# NAVAL POSTGRADUATE SCHOOL

## MONTEREY, CALIFORNIA

# THESIS

PERFORMANCE CHARACTERIZATION OF SWEPT RAMP OBSTACLE FIELDS IN PULSE DETONATION APPLICATIONS

by

William T. Dvorak

March 2010

Thesis Advisor:                Christopher M. Brophy
Second Reader:               Anthony J. Gannon

**Approved for public release; distribution is unlimited**

THIS PAGE INTENTIONALLY LEFT BLANK

| REPORT DOCUMENTATION PAGE | | *Form Approved OMB No. 0704-0188* |
|---|---|---|
| Public reporting burden for this collection of information is estimated to average 1 hour per response, including the time for reviewing instruction, searching existing data sources, gathering and maintaining the data needed, and completing and reviewing the collection of information. Send comments regarding this burden estimate or any other aspect of this collection of information, including suggestions for reducing this burden, to Washington headquarters Services, Directorate for Information Operations and Reports, 1215 Jefferson Davis Highway, Suite 1204, Arlington, VA 22202-4302, and to the Office of Management and Budget, Paperwork Reduction Project (0704-0188) Washington DC 20503. | | |
| **1. AGENCY USE ONLY** *(Leave blank)* | **2. REPORT DATE** March 2010 | **3. REPORT TYPE AND DATES COVERED** Master's Thesis |
| **4. TITLE AND SUBTITLE** Performance Characterization of Swept Ramp Obstacle Fields in Pulse Detonation Applications | | **5. FUNDING NUMBERS** |
| **6. AUTHOR(S)** William T. Dvorak | | |
| **7. PERFORMING ORGANIZATION NAME(S) AND ADDRESS(ES)** Naval Postgraduate School Monterey, CA 93943-5000 | | **8. PERFORMING ORGANIZATION REPORT NUMBER** |
| **9. SPONSORING /MONITORING AGENCY NAME(S) AND ADDRESS(ES)** N/A | | **10. SPONSORING/MONITORING AGENCY REPORT NUMBER** |
| **11. SUPPLEMENTARY NOTES** The views expressed in this thesis are those of the author and do not reflect the official policy or position of the Department of Defense or the U.S. Government. IRB Protocol number _____, | | |
| **12a. DISTRIBUTION / AVAILABILITY STATEMENT** Approved for public release; distribution is unlimited | | **12b. DISTRIBUTION CODE** |

**13. ABSTRACT (maximum 200 words)**

Pulse Detonation technology offers the potential for substantial increases in thrust and fuel efficiency in subsonic and supersonic flight Mach ranges through the use of a detonative vs. deflagrative combustion process. One of the approaches to reliably obtain a fuel-air detonation is to accelerate a deflagration combustion wave to detonation through the use of turbulence devices, known as detonation-to-deflagration transition. Current geometries for deflagration-to-detonation transition sacrifice much of the gains through losses from high velocity flows over obstacle fields required for detonation initiation. In this study, experimental swept ramp obstacle fields were characterized in an effort to realize decreased pressure losses while still creating the gas dynamic and turbulence necessary for detonation initiation. Characterization included measurement of pressure loss across the combustor during "cold flow" operation with no ignition or fuel present, and detonability testing that employed ion probe measurement of combustion wave velocity. Minimizing pressure losses existing in current designs will result in dramatic improvement of system performance.

In addition to swept ramp fields, other configurations were analyzed using computational fluid dynamics (CFD) and subjected to performance testing. Of particular interest were obstacles of similar blockage area, but without the swept sides associated with streamwise vorticity in the flow field. Testing of unswept configurations allowed insight into the mechanisms for DDT and narrowed the field of practical obstacle geometries.

| **14. SUBJECT TERMS** Pulse Detonation, PDE, Transient Plasma Ignition, TPI, Swept Ramp Obstacles, CFD, Ion Probe Measurement, Pressure Loss | | | **15. NUMBER OF PAGES** 97 |
|---|---|---|---|
| | | | **16. PRICE CODE** |
| **17. SECURITY CLASSIFICATION OF REPORT** Unclassified | **18. SECURITY CLASSIFICATION OF THIS PAGE** Unclassified | **19. SECURITY CLASSIFICATION OF ABSTRACT** Unclassified | **20. LIMITATION OF ABSTRACT** UU |

THIS PAGE INTENTIONALLY LEFT BLANK

**PERFORMANCE CHARACTERIZATION OF SWEPT RAMP OBSTACLE
FIELDS IN PULSE DETONATION APPLICATIONS**

William T. Dvorak
Lieutenant, United States Navy
B.S., University of Arizona, 2002

Submitted in partial fulfillment of the
requirements for the degree of

**MASTER OF SCIENCE IN ASTRONAUTICAL ENGINEERING**

from the

**NAVAL POSTGRADUATE SCHOOL
March 2010**

Author:　　　　　　William T. Dvorak

Approved by:　　　　Christopher M. Brophy
　　　　　　　　　　Thesis Advisor

　　　　　　　　　　Anthony J. Gannon
　　　　　　　　　　Second Reader

　　　　　　　　　　Knox T. Millsaps
　　　　　　　　　　Chairman, Department of Mechanical and Aerospace Engineering

THIS PAGE INTENTIONALLY LEFT BLANK

# ABSTRACT

Pulse Detonation technology offers the potential for substantial increases in thrust and fuel efficiency in subsonic and supersonic flight Mach ranges through the use of a detonative vs. deflagrative combustion process. One of the approaches to reliably obtain a fuel-air detonation is to accelerate a deflagration combustion wave to detonation through the use of turbulence devices, known as detonation-to-deflagration transition. Current geometries for deflagration-to-detonation transition sacrifice much of the gains through losses from high velocity flows over obstacle fields required for detonation initiation. In this study, experimental swept ramp obstacle fields were characterized in an effort to realize decreased pressure losses while still creating the gas dynamic and turbulence necessary for detonation initiation. Characterization included measurement of pressure loss across the combustor during "cold flow" operation with no ignition or fuel present, and detonability testing that employed ion probe measurement of combustion wave velocity. Minimizing pressure losses existing in current designs will result in dramatic improvement of system performance.

In addition to swept ramp fields, other configurations were analyzed using computational fluid dynamics (CFD) and subjected to performance testing. Of particular interest were obstacles of similar blockage area, but without the swept sides associated with streamwise vorticity in the flow field. Testing of unswept configurations allowed insight into the mechanisms for DDT and narrowed the field of practical obstacle geometries.

THIS PAGE INTENTIONALLY LEFT BLANK

# TABLE OF CONTENTS

viii

# LIST OF FIGURES

# LIST OF TABLES

THIS PAGE INTENTIONALLY LEFT BLANK

# LIST OF ACRONYMS, ABBREVIATIONS, AND SYMBOLS

| | | |
|---|---|---|
| C-J | - | Chapman-Jouguet |
| CAD | - | Computer-Aided Design |
| CCD | - | Charge-Coupled Device |
| CFD | - | Computational Fluid Dynamics |
| CMOS | - | Complementary Metal–Oxide–Semiconductor |
| CPU | - | Central Processing Unit |
| CEQUEL | - | Chemical Equilibrium in Excel |
| DDT | - | Deflagration-To-Detonation Transition |
| NI | - | National Instruments |
| NPS | - | Naval Postgraduate School |
| PDC | - | Pulse Detonation Combustor |
| PDE | - | Pulse Detonation Engine |
| RAM | - | Random Access Memory |
| RDT | - | Research, Design and Test |
| RPL | - | Rocket Propulsion Laboratory |
| STP | | Standard Temperature and Pressure |
| USB | - | Universal Serial Bus |
| VI | - | Virtual Instrument |
| VIS | - | Variable Ignition System |
| ZND | - | Zeldovich–Neumann–Döring |
| $A$ | - | Area ($m^2$) |
| C | - | carbon |
| $C_2H_4$ | - | ethylene |
| $c$ | - | speed of sound (m/s) |
| $c_P$ | - | constant pressure coefficient of specific heat (J/kgK) |
| cm | - | centimeter |
| $f$ | - | fuel-to-air ratio  [dimensionless] |
| GB | - | gigabyte |
| GHz | - | gigahertz |
| $g$ | - | gravitational constant |

| | | |
|---|---|---|
| H | - | hydrogen |
| K | - | Kelvin |
| kg | - | kilogram |
| MHz | - | megahertz |
| m | - | meter |
| mm | - | millimeter |
| $M$ | - | Mach number |
| MB | - | Megabyte |
| Mb | - | Megabit |
| $\dot{m}$ | - | mass flow rate (Kg/s) |
| $\dot{m}_f$ | - | mass flow rate of fuel (Kg/s) |
| $\dot{m}_a$ | - | mass flow rate of air (Kg/s) |
| $\dot{m}_{tot}$ | - | total mass flow rate (Kg/s) |
| N | - | nitrogen |
| O | - | oxygen |
| $p$ | - | pressure (psi) |
| psi | - | pounds per square inch |
| psig | - | pounds per square inch gage |
| $P\text{-}v$ | - | pressure-specific volume |
| $q$ | - | specific heat |
| $R$ | - | specific gas constant |
| s | - | second |
| $s$ | - | entropy |
| $t$ | - | time (s) |
| $T$ | - | temperature (K) |
| $u$ | - | velocity (m/s) |
| $V_{det}$ | - | Detonation Velocity (m/s) |
| v | - | velocity (m/s) |
| $\phi$ | - | equivalence ratio [dimensionless] |
| $\gamma$ | - | specific heat ratio [dimensionless] |
| $\rho$ | - | density (kg/m$^3$) |

# ACKNOWLEDGMENTS

THIS PAGE INTENTIONALLY LEFT BLANK

# I.    INTRODUCTION

Pulse detonation engines (PDE) continue to be explored due to the inherent thermodynamic advantages of a near-constant volume or detonative combustion cycle [1]. The application of detonation-based combustion has been proposed in a variety of concepts, ranging from basic "pure" PDE systems for low-cost high-speed propulsion to hybrid gas-turbine systems. The hybrid gas-turbine systems have an increased benefit from the replacement of the costly high-pressure spool with a pressure-gain combustor utilizing a detonation process that could be used for either ground-based power generation or propulsive purposes [2–5]. The basic PDE system has often been depicted as being composed of a valve, combustors, and either a single or individual nozzle arrangement. Both architectures rely on the continued development and demonstration of technologies which produce reliable ignition and effective detonation initiation [6–8] in practical hydrocarbon mixtures. Many of the analytical papers and articles detailing the thermodynamic advantages of detonation-based combustion often assume that the detonability process for practical hydrocarbon fuels is readily achieved and done so with great efficiency. Practically, this is rarely the case, since most of the historic efforts pertaining to pulse detonation systems utilized either high-energy initiators [5, 6], Shchelkin spirals (Figure 1), or obstacles with substantial blockage ratios [2, 9] to initiate deflagration to detonation transition (DDT).



FLOW
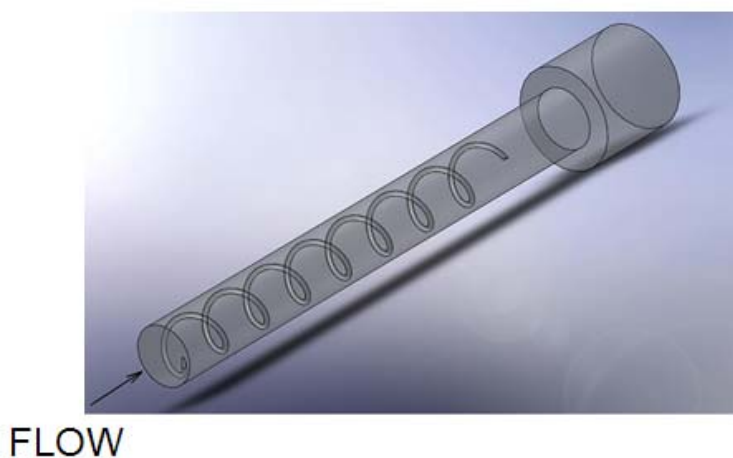
Figure 1.     Shchelkin spiral combustor obstacle

The use of explosive material or high-energy initiators to initiate DDT in fuel/air mixtures is simply impractical for any system operating over thousands of cycles. Early research into "pre-detonators" demonstrated that fuel/oxygen mixtures could be easily initiated in a smaller combustor and then reliably transmitted into a fuel/air mixture through geometry discontinuities [10, 11], but was deemed impractical from a system-level point of view. The common approach to initiate DDT in PDE combustors which has seen the most utilization has been a Shchelkin-like wall spiral [12–14], wall turbulence devices and of the variants available.

Most of the spiral turbulence devices that have been evaluated by investigators in the past, possessed a noticeable total pressure loss during both the filling and detonation portion of the cycle [15, 16], but were not often reported. Generally, the goal of most previous efforts was to develop ways to initiate a detonation in as short of a distance as possible and not necessarily be concerned with practical engine cycle issues. These losses can be substantial during the refresh portion of the engine cycle, which typically accounts for about 60% cycle time. The associated penalties are inherently amplified with increasing Mach refresh numbers. The total pressure losses continue to be present during the detonation and blow down portion of the cycle, and although short in duration, can also generate a large portion of the overall system inefficiencies due to the increased velocities, viscosities, and turbulence losses experienced by the combustion products. An additional concern when using spiral devices is the highly dynamic mechanical loads generated throughout the operating cycle and the associated thermal management issues that can occur at moderate operational frequencies, such as 40–80Hz. The thermal loads on the spiral devices not only present a difficult challenge in terms of the required cooling for increased longevity, but also introduce an additional loss mechanism into the engine cycle since they add and subtract heat from the working fluid at inappropriate times during the PDE cycle [17]. The spiral devices, which are effectively suspended in the flow, "heat soak" during the cycle. The incoming "fresh" fuel/air charge is then inadvertently preheated through the cycle, which removes energy from the working fluid and decreases the energy density of the mixture.
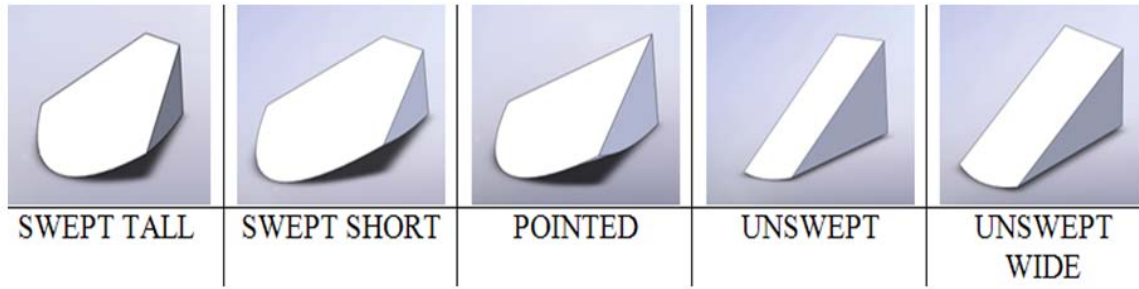
Figure 2. Ramp obstacles tested

The modular swept-ramp obstacles, shown in Figure 2, possess two favorable characteristics: substantially lower total pressure loss associated with streamwise vorticity/mixing and the associated small scale turbulence generated by instabilities associated with rotational flows, especially in the presence of large flow anisotropy and distributed combustion zones. Previous work by Lindstedt and Michels [18, 19] revealed how large flow gradients and flame/vortex interactions can result in a dramatic increase in turbulence levels and decrease in turbulence length scales. The effective flame front surface increases at a high rate and can ultimately result in an explosion event if proper conditions exist. These conditions are driven by large flow gradients in the axial direction which increase further with each explosion event, thus producing a series of explosion events at predictable locations. The swept ramp obstacles provide controlled production of these explosion events while preserving a low total pressure loss for the aggregate flow.

THIS PAGE INTENTIONALLY LEFT BLANK

# II.  BACKGROUND

## A.  MOTIVATION

Constant pressure combustion processes are employed in the majority of modern propulsion systems (gas turbine, diesel).  These systems are well understood and refined, but are reaching the pinnacle of their efficiency.  Industry devotes large amounts of research capital to funding modest increases in performance of these systems.  In order to achieve substantial improvements, alternate approaches are being explored.  Constant volume combustion processes offer theoretically higher thermodynamic efficiencies.  While systems employing this mode of combustion are not as mature as their constant pressure counterparts, continuing research efforts are attempting to advance and apply this technology.  The following chapter provides a background and foundation for the research conducted in this work.

## B.  COMBUSTION PROCESSES

Propulsion engines can be classified according to the type of combustion process they employ.  The vast majority utilizes a deflagration combustion process, but this thesis explores detonation based combustion exclusively.  The following paragraphs delineate the two modes of combustion and introduce several other concepts critical to understanding the detonation phenomenon and the efficient extraction of useful work from it.

### 1.  Deflagration

Deflagration refers to combustion waves propagating at subsonic velocities.  This is the most common mode of combustion, and it is present in turbo machinery and conventional rocket engines.  As the combustion wave propagates through a fuel/air mixture, the energy released is added to the working fluid in the form of a temperature rise by way of thermal diffusion.  This continues the combustion, but limits the propagation to subsonic speeds. The temperature and pressure of the reactants affect the rate at which reactants are consumed as well, which further affects the speed at which

combustion occurs.  Introducing turbulence to the flow field increases the surface area of the flame front and can increase the burn rate of the unreacted mixture.

### 2.    Detonation

Detonation is an energetic process that is characterized by supersonic combustion velocities.  The motion of the shockwave relative to the unburned fuel/air mixture is supersonic and compresses the mixture substantially.  This compression raises the pressure, temperature, and density until a violent exothermic reaction occurs.  The reaction further energizes the combustion front in a positive feedback loop that becomes self sustaining.  Due to the extreme speed at which the reaction occurs, the process is considered constant volume.

### 3.    Differences between Detonation and Deflagration

A qualitative comparison of the two modes of combustion is necessary to gain insight into the performance implications.  Figure 3 illustrates the motion of a one-dimensional planar combustion wave in a long duct with constant cross sectional area.  In this frame of reference, the combustion wave is held stationary and unburned reactants approach the wave from the left with velocity $u_1$. Burned reactants move away from the stationary wave to the right with velocity $u_2$.
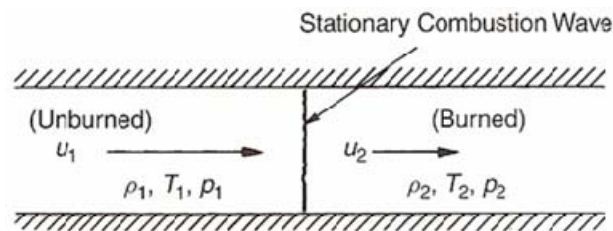


Figure 3.    Schematic diagram of stationary 1-D combustion wave [From 1]

The type of combustion wave has an enormous effect on the property changes of the mixture.  Table 1 summarizes the ratio of critical velocities ($u_{1,2}$), densities ($\rho_{1,2}$), temperatures($T_{1,2}$), and pressures of the burned and unburned mixtures.  The most important difference between the two columns is the contrast between pressures and

temperatures. The detonation process increases temperature while also compressing the mixture, resulting in higher enthalpies than the deflagration process which allows a slight expansion.

|  | Detonation | Deflagration |
|---|---|---|
| $u_1/c_1$ | 5-10 | 0.0001-0.03 |
| $u_2/u_1$ | 0.4-0.7 (deceleration) | 4-16 |
| $p_2/p_1$ | 13-55 (compression) | 0.98-0.976 (slight expansion) |
| $T_2/T_1$ | 8-21 (heat addition) | 4-16 (heat addition) |
| $\rho_2/\rho_1$ | 1.4-2.6 | 0.06-0.25 |

Table 1.    Thermodynamic property ratios for detonation vs. deflagration [From 1]

## C.    DETONATION THEORY

A convenient way to gain understanding of the one-dimensional model in the previous section is discussion of the Hugoniot curve. The Hugoniot curve is a plot of pressure and specific volume that results from any given initial pressure and specific volume. Points on the curve are theoretical post combustion states, although not all are physically attainable.

Listed below are the conservation equations for steady one-dimensional flow, with no body forces or external heat addition or loss.

Conservation of Mass:    $\rho_1 u_1 = \rho_2 u_2$    (1)

Conservation of Momentum:    $p_1 + \rho_1 u_1^2 = p_2 + \rho_2 u_2^2$    (2)

Conservation of Energy:    $h_1 + \dfrac{1}{2}u_1^2 = h_2 + \dfrac{1}{2}u_2^2$    (3)

For a constant area problem, Equation (1) illustrates that mass flow rate ($\dot{m}$) must be constant and when combined with Equation (2) yields the Raleigh-line relation below Equation (4). The slope of the Raleigh-Line indicates the velocity of the detonation wave.

Raleigh-Line Relation:
$$\rho_1^2 u_1^2 = \frac{p_2 - p_1}{\dfrac{1}{\rho_1} - \dfrac{1}{\rho_2}} = \dot{m}^2 \qquad (4)$$

The Hugoniot Relation is obtained by manipulating the Raleigh-Line relation of Equation (4) through substitution of Equation (3), and introducing specific heat ($c_p$).

$$c_p = \frac{\gamma}{\gamma - 1} R \qquad (5)$$

When the resulting equation is solved for $q$, it yields a form that eliminates the velocity conditions $u_1$ and $u_2$. The final equation (6) relates final pressure and specific volume to the initial pressure ($p_1$) and specific volume for a given heat release per unit mass ($q$).

Hugoniot Relation:
$$\frac{\gamma}{\gamma - 1}\left(\frac{p_2}{\rho_2} - \frac{p_1}{\rho_1}\right) - \frac{1}{2}(p_2 - p_1)\left(\frac{1}{\rho_1} + \frac{1}{\rho_2}\right) = q \quad (6)$$

Figure 4 shows the Hugoniot Curve. There are five possible regions on the curve, which describe theoretical combustion conditions. These regions are described by construction from an origin A ($p_1, 1/\rho_1$). Tangent lines drawn from the origin A represent the Rayleigh Solution and locate the Upper and Lower Chapman-Jouguet Points at each tangency.
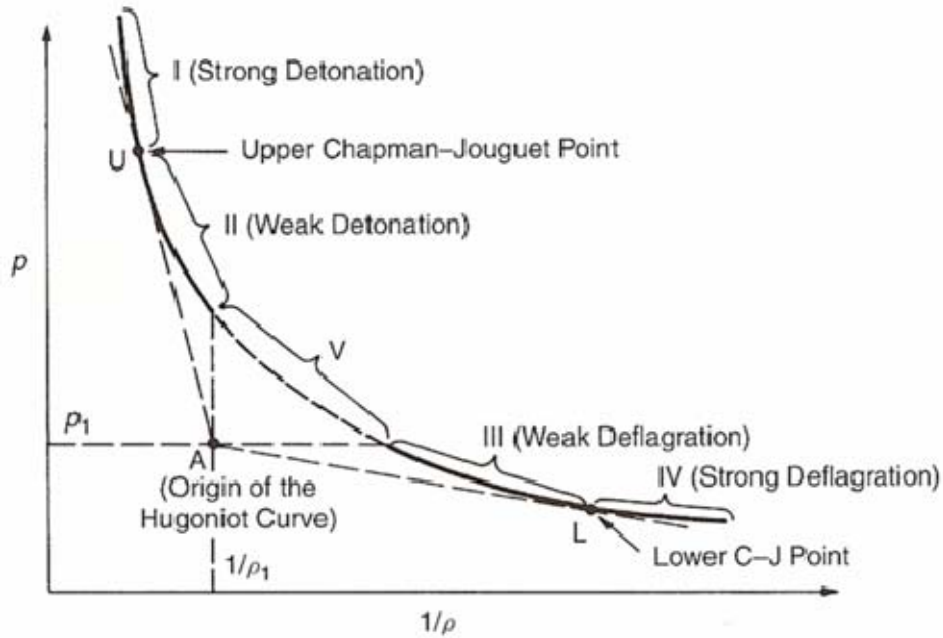
Figure 4.    Theoretical regions of the Hugoniot curve [From 1]

Constant pressure and specific volume lines drawn from the origin further delineate the curve and complete the creation of combustion regions I-V. All of the regions, while mathematically possible, are not observed; Region V is physically impossible, as it requires $p_2 > p_1$ and $1/\rho_2 > 1/\rho_1$. This represents a simultaneous increase in pressure while density decreases, resulting in an imaginary velocity of $u_1$ in the Rayleigh-Line Relation of Equation (4).

Regions I and II are transient in nature, and tend to quickly stabilize towards the upper C-J point, U. Region I is the strong detonation region since $p_2 > p_{\text{upper C-J}}$. It requires a strong overdriven shock, and seldom observed. Region II is called the weak detonation region and requires exceptionally fast chemical kinetics. Region IV is the strong deflagration region, and is not an attainable steady-state solution in a constant area duct as it requires an acceleration to supersonic velocities (not possible). Having ruled out all other regions, only weak deflagration (region III) and detonations stabilizing at the Upper C-J point are practical.

Burned products from detonation combustion travel away from the shock wave at sonic velocity for the upper C-J point. This is proven by solving the Hugoniot Relation for $p_2$ and differentiating with respect to specific density $(1/\rho_2)$. The result is the slope of the curve, Equation (7):

$$\text{Slope of the Hugoniot Curve: } \frac{dp_2}{d(1/\rho_2)} = \frac{(p_2 - p_1) - \left(\frac{2\gamma}{\gamma-1}\right)p_2}{\left(\frac{2\gamma}{\gamma-1}\right)\frac{1}{\rho_2} - \left(\frac{1}{\rho_1} + \frac{1}{\rho_2}\right)} \qquad (7)$$

Evaluating equation (7) at the upper or lower C-J points yields Equation (8):

$$\text{Slope at upper or lower C-J Point: } \frac{dp_2}{d(1/\rho_2)} = \frac{p_2 - p_1}{1/\rho_2 - 1/\rho_1} = V_{det} \qquad (8)$$

Combined with the Rayleigh-Line Relation of Equation (4):

$$\text{Velocity at C-J Points: } u_2^2 = \frac{\gamma p_2}{\rho_2} = c_2^2 \qquad (9)$$

Since $u_2 = c_2$, the velocity of the burned reactants is equal to the local speed of sound relative to the detonation wave for either deflagration or detonation at the upper and lower C-J points.

## D.    THERMODYNAMIC ADVANTAGES OF DETONATIONS

Several factors contribute to the increased theoretical efficiency of detonation combustion. First is the increased work that can be extracted from the Humphrey cycle as opposed to the more traditional Brayton cycle. Detonation events also introduce a lower entropy rise to a system during combustion. Both the cycle efficiency and decreased entropy addition are detailed below.

### 1.    Increased Cycle Efficiency of Pulse Detonation Engines

Pulse detonation engines differ from typical air breathing engines that rely on steady state deflagration. The discrete periodic detonations occur over very short timescales, and are considered a nearly constant volume process. Traditional processes

utilize constant pressure combustion, and an examination of a pressure-volume diagram illustrates the advantage of detonation based cycles. The traditional Brayton cycles is shown in Figure 5 along with a Humphrey (PDE) cycle.
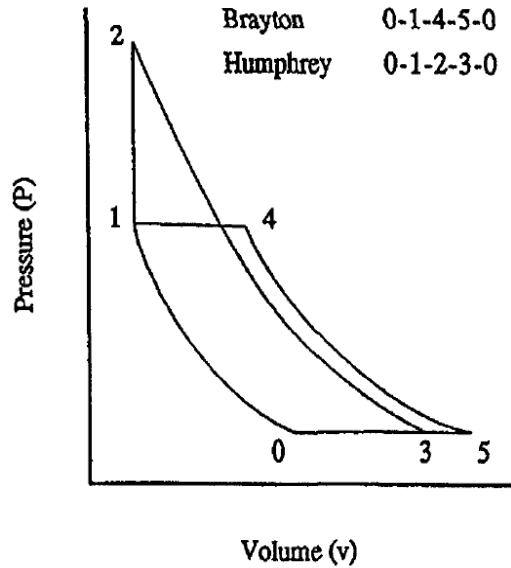


Figure 5.     Pressure-volume cycle diagram of pulse detonation engine [From 7]

The two cycles are similar, except the isobaric (1–4) combustion of the Brayton cycle is replaced with a vertical constant volume process (1–2). Integration of Pressure with respect to volume yields the work of either cycle, and it is obvious from the diagram that the detonation curve encloses more area for a similar heat addition.

## 2.     Lower Entropy Addition of Detonation Combustion Events

An excessive entropy rise during a process can be viewed as a measure of the useful energy lost during the process. It follows logically that a thermodynamic event which results in a lower entropy rise for a system for the same energy addition will be capable of extracting more useful work. Figure 6 displays the entropy values for each region along the Hugoniot curve. The maximum value of entropy on this diagram corresponds to the lower Chapman-Jouguet point. The entropy addition at the lower C-J point is much higher than the minimum value associated with the upper C-J point that

represents detonation events. Entropy addition from weak deflagration (lower C-J) can be minimized by decreasing specific volume or increasing pressure, but can not approach the thermodynamic efficiency of detonations.
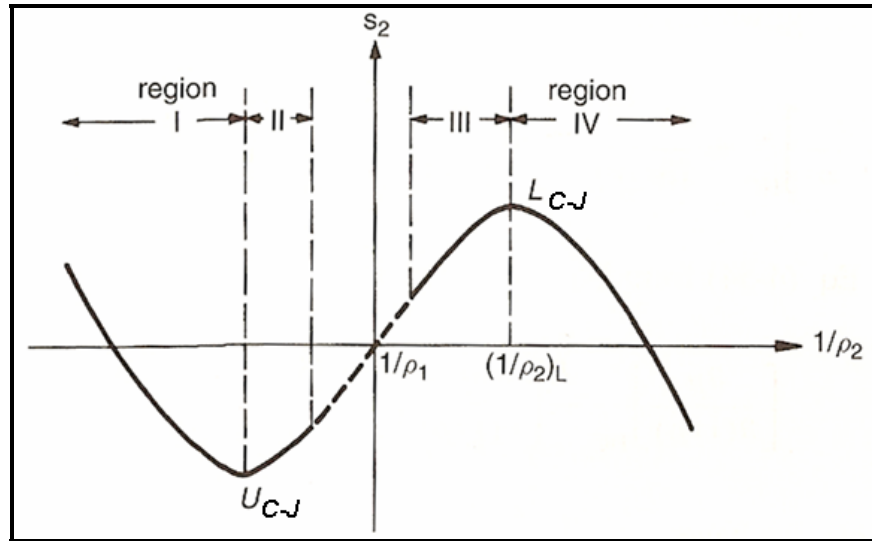


Figure 6.    Entropy distribution on the Hugoniot curve [From 1]

## E.    DEFLAGRATION-TO-DETONATION TRANSITION

Several methods exist for initiating detonations.  Extremely high energy direct initiation and Deflagration-to-Detonation transition (DDT) are the two primary methods. Ground-based systems may have the engineering margin to utilize high-energy direct initiation, but smaller tactical systems require a less massive and simpler solution. Missile propulsion must be reliable, robust, and capable of operating at high frequencies. Deflagration-to-Detonation Transition is capable of achieving these requirements.
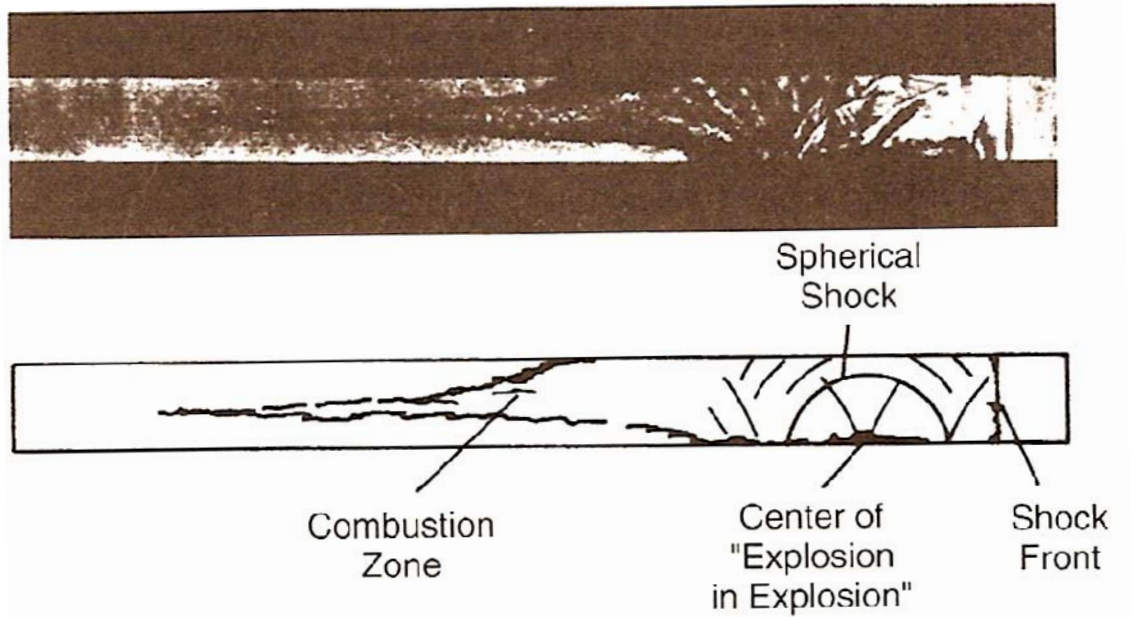
Figure 7.    Small explosion (detonation precursor) events in DDT [From 1]

DDT begins with a deflagration wave initiated in a reactive mixture by way of a low energy ignition source.  As the deflagration wave proceeds down a confined area, pressure waves propagate ahead of the flame at sonic velocities.  These pressure waves create turbulent conditions ahead of the flame, which increase the surface area of the front, and further amplify the reaction rates of the combusting mixture.  A feedback is established where the turbulence increases the reaction rates, which in turn further increases the turbulence.  When this process achieves adequate energies, small explosions (Figure 7) can be observed which rapidly accelerate the surrounding gas and merge with the initial shock.  This creates transverse waves and a retonation wave that is reflected back into the burned mixture.  As these multiple shock waves (Figure 8) propagate and begin to interact with each other, a final steady detonation wave is created at the C-J detonation velocity.
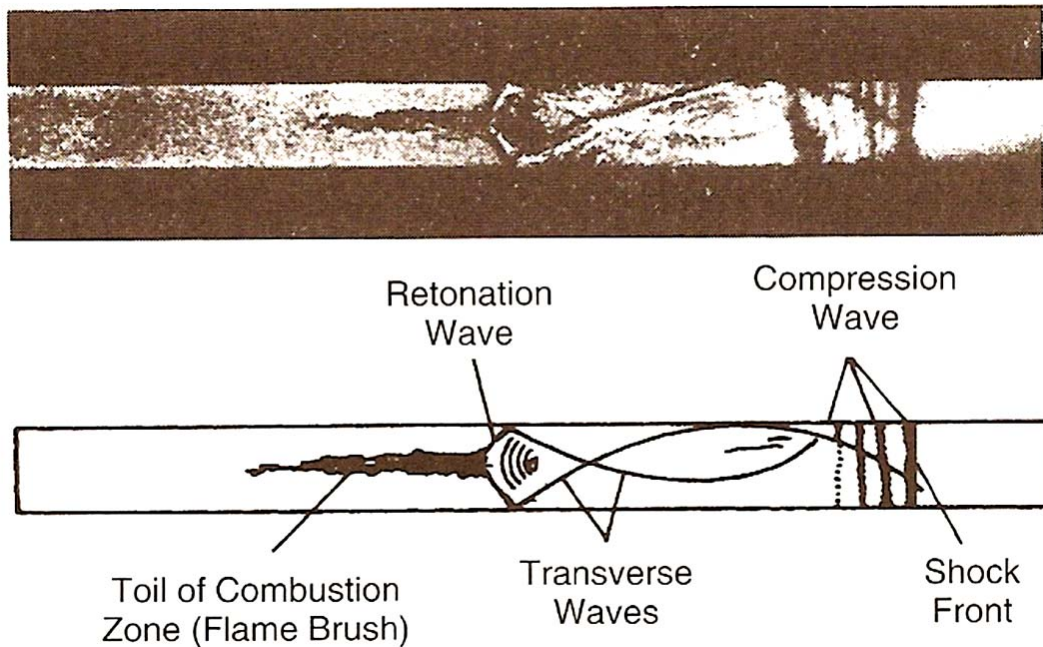
Figure 8.    DDT transverse and retonation waves [From 1]

## F.    OBSTACLE FIELD DDT ACCELERATION

Deflagration-to detonation can occur in tubes without obstacles given sufficient length due to wall roughness and the resulting turbulence introduction.  While possible, the smooth tube DDT can require combustor lengths that are an order of magnitude greater than those with obstacles [20].  Obstacle fields such as the one shown in Figure 9 accelerate the DDT process, and achieve significantly shorter detonation run-up distances.  In addition to decreasing the length required, obstacle fields increase the repeatability of the DDT process.  In a smooth tube, the transition from deflagration is statistical and heavily dependent on tube wall effects.   Introduction of obstacles dominates the tube wall roughness effects, and the results become largely independent of other details of the apparatus.  Although obstacle fields foster repeatability and shorten transition lengths, the drawback is pressure loss across the tube.

14

Weak ignition and slow flame propagation

Flame folding and onset of turbulence

Obstacles

Turbulent flame acceleration and shock formation

Onset of detonation

DDT or run-up distance

Propagation of detonation
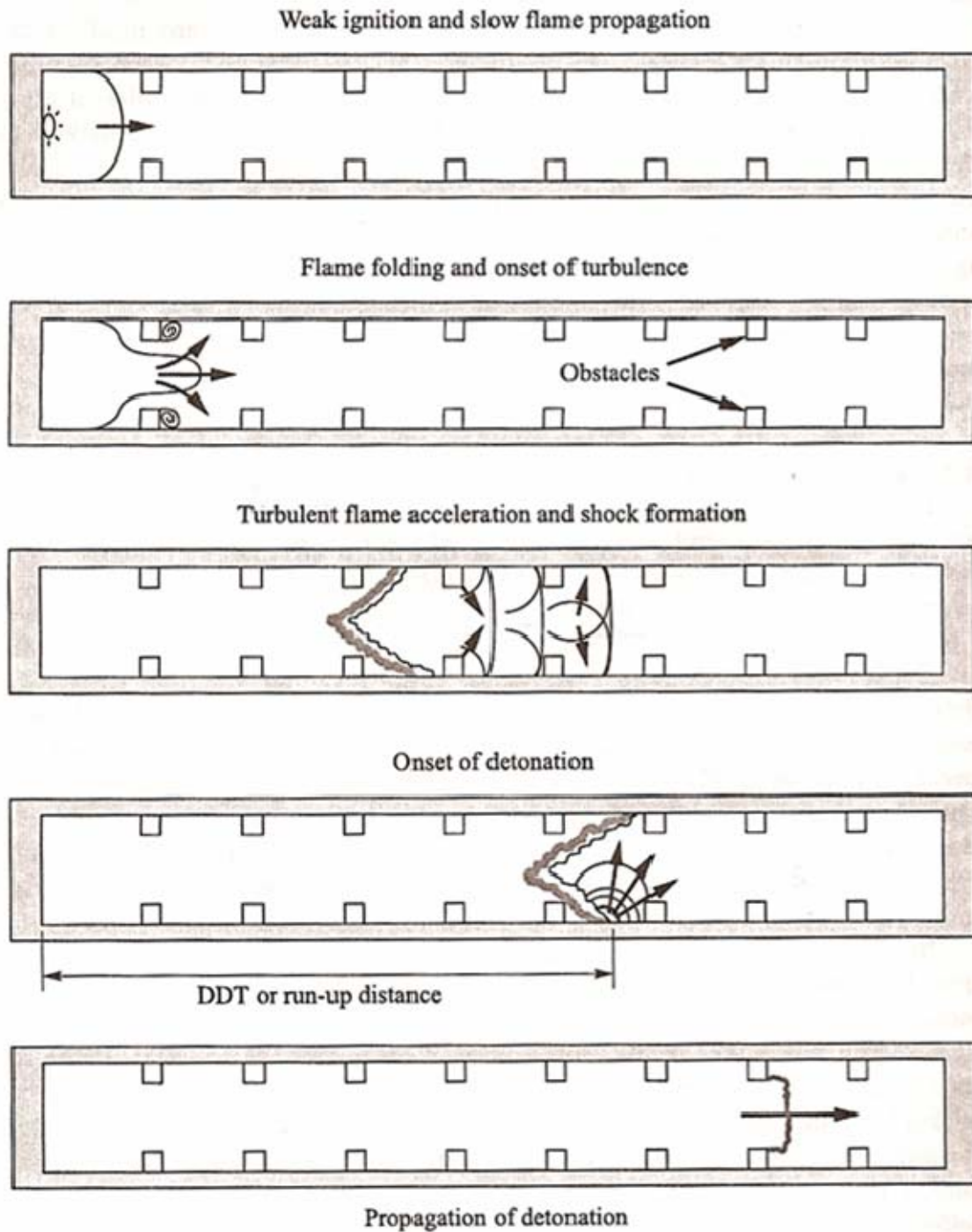
Figure 9.     DDT acceleration in a tube with obstacles [From 20]

15

## G.    PULSE DETONATION ENGINES

Figure 10 is an illustration of one cycle of a Pulse Detonation Engine.  The first step is to inject air and fuel (controlled by a solenoid valve) into the head end of the combustor (1).  Once a predefined amount of the tube is filled with the reactive mixture (2), it is ignited (3).



| | |
|---|---|
| 1.  Reactants injected | 5.  Detonation wave exits |
| 2.  Tube fills | 6.  Rarefaction waves |
| 3.  Mixture ignited | 7.  Products exhausted |
| 4.  Detonation wave forms | 8.  Cycle repeats |
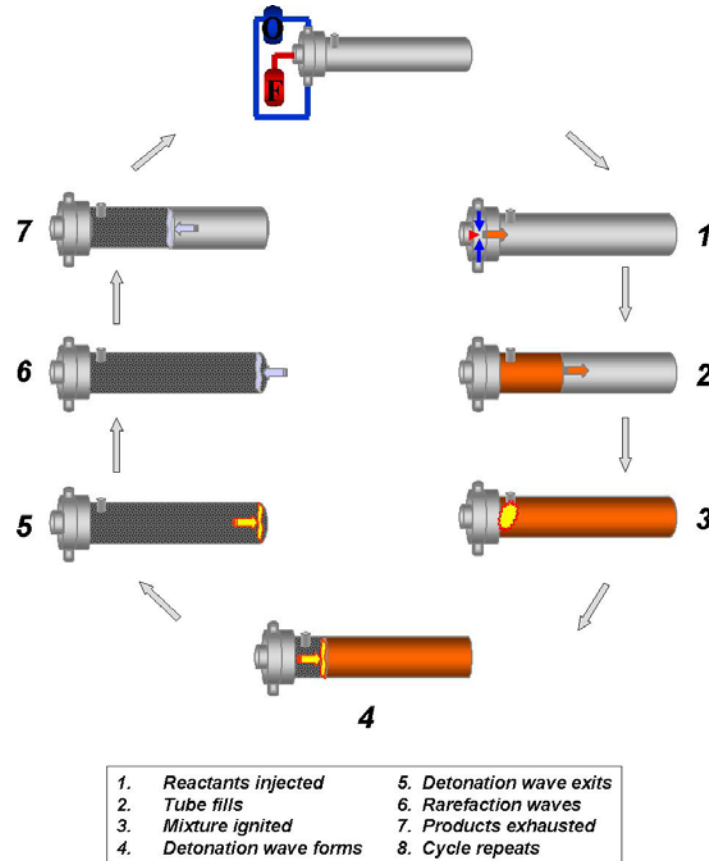
Figure 10.    Single PDE cycle [From 21]

The initial deflagration wave propagates down the tube (4) until DDT is achieved (5).  The supersonic detonation wave burns the remaining reactants and the remaining gases are then evacuated out of the tube, which results in thrust (7).  Following the shock wave exit, continued air flow through the tube purges any remaining products.  The cycle is then repeated (8).  Since the thrust from this engine is not continuous, every effort is made to minimize the blowdown (purge) portion of the cycle.   This requirement necessitates high frequency operation for practical thrust extraction.

# III.  COMPUTER SIMULATION

## A.  MOTIVATION

Prior to conducting any physical testing of combustor configurations, computer modeling was employed to gain understanding of flow field conditions.  Due to the extremely complex chemical interactions involved in the detonation process, computer models are not expected to fully predict experimental outcomes exactly.  While the computational outcomes were not relied upon solely, the simulations conducted were valuable as an indicator for promising configurations.  The mechanism for DDT is enigmatic in general, and the process was less understood for the obstacle fields in this study.  With this in mind, it was decided the best course of action was to model the flow fields and look for trends common to the configurations that resulted in a successful DDT event.  This qualitative approach allows the computational analysis to be used as a stepping stone toward physical component testing.

## B.  MODELING SOFTWARE

Two different software suites were used in the formation and evaluation of these computer models.  Models were created using SolidWorks 2008.  SolidWorks is a 3-D computer-aided design program for Windows developed by Dassault Systems Corp. in France.  It creates parasolid models that are imported into ANSYS Workbench (meshing and computational fluid dynamics (CFD) solver).  Specifically, CFX 12.0 pre and post are the elements of ANSYS workbench that handled the processing and display of results, respectively.

### 1.  Parasolid Creation

As mentioned above, SolidWorks was used to create the parasolid model.  First, the individual ramps were built using various sketch and extrusion operations.  Once the ramp model was complete, it was duplicated and mated to the inside of a virtual 24" combustor tube with a 3" diameter.  The flanged tube and ramp are displayed in Figure 11, and detailed drawings of all components are included in Appendix C.  Each

combustor has locations for ramp placement at 3" (one diameter) increments down the length of the tube. Each of these spots is called a station. The nomenclature #R.###.#S was developed for use throughout this analysis for differentiating configurations. The first # is the number of ramps at each axial station, followed by the three digit angular separation of the ramps in each station. The final # is the number of stations. This alphanumeric is followed by a description of what type of ramp was employed for each configuration. The labeling system is maintained for the experimental physical testing as well. Examples of each type of configuration are tabulated in Appendix A.
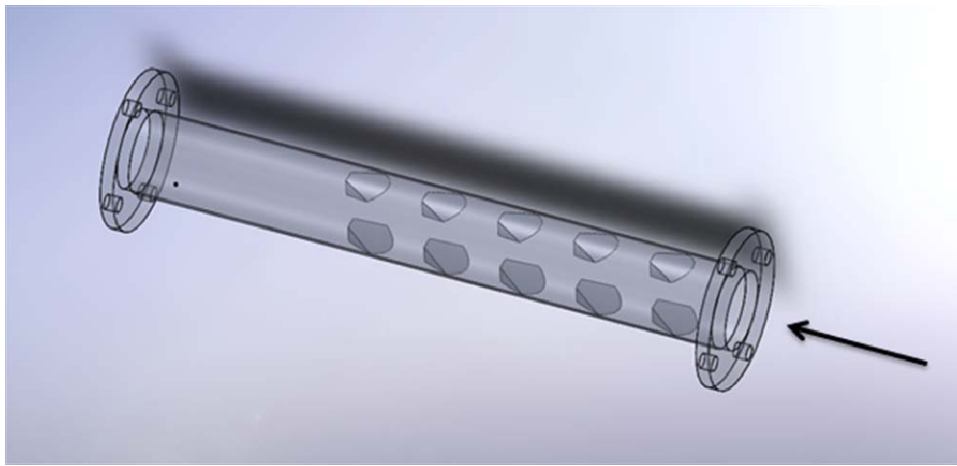


Figure 11.    Parasolid model of combustor tube and swept ramps

### 2.    Meshing and Simulation

Meshing was accomplished using the ANSYS workbench utility. The number of nodes and elements for each relevant simulation described are listed in Table 2. It is important to note that many configurations were evaluated computationally, but only those necessary to illustrate mechanisms of successful and unsuccessful combustor sections are discussed. An example of a meshed combustor section is shown in Figure 12.

| Configuration | No of Nodes | No of Elements |
|---|---|---|
| 2R.180.5S unswept | 2,307,322 | 8,970,289 |
| 2R.180.5S swept | 2,232,666 | 8,842,289 |
| 4R.090.5S swept | 2,262,504 | 8,826,352 |

Table 2.    Relevant configurations evaluated computationally
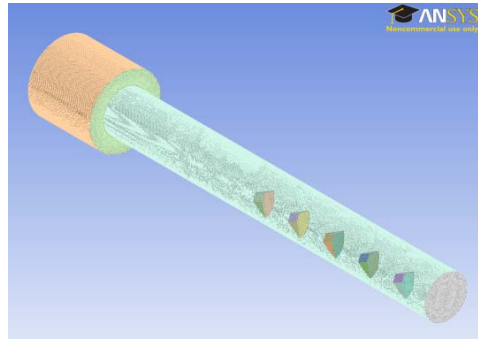


Figure 12.    Mesh of 2R.180.5S model with 8,842,289 elements

## C.    SIMULATION SUMMARY

Computational Analysis was limited to steady state flow field studies. Two swept ramp and one "straight" ramp configurations were explored. All simulations had identical initial and boundary conditions with the exception of ramp configuration. A summary of all computational boundary conditions is contained in Table 3.

| Location | Type | Conditions | |
|---|---|---|---|
| Inlet | Inlet | Flow Direction:<br>Flow Regime:<br>Heat Transfer:<br>Static Temperature:<br>Mass Flow Rate:<br>Mass And Momentum:<br>Turbulence: | Normal to Boundary Condition<br>Subsonic<br>Static Temperature<br>275[K]<br>0.3125 [kg/ s]<br>Mass Flow Rate<br>Medium Intensity  (5%) |
| Outlet | Outlet | Flow Regime:<br>Mass And Momentum:<br>Pressure Profile Blend:<br>Relative Pressure:<br>Pressure Averaging: | Subsonic<br>Average Static Pressure<br>0.05<br>0 [Pa]<br>Average Over Whole Outlet |
| Wall | Wall | Heat Transfer:<br>Mass And Momentum:<br>Wall Roughness: | Adiabatic<br>No Slip Wall<br>Rough Wall |
| Exit Volume Front | Opening | Flow Regime:<br>Mass And Momentum:<br>Opening Temperature:<br>Relative Pressure:<br>Turbulence | Subsonic<br>Entrainment<br>298 [K]<br>0 [Pa]<br>Zero Gradient |
| Exit Volume Side | Wall | Heat Transfer:<br>Mass And Momentum: | Adiabatic<br>Free Slip Wall |

Table 3.    Tabulation of initial and boundary conditions

The three discussed geometries were chosen to demonstrate characteristics common to flow field solutions of each type.  All three cases display flow conditions at a perpendicular plane just preceding the end of the 5$^{th}$ stage.  The position of this plane is detailed in Figure 13.  This plane was chosen to highlight the obstacles effect on the flow field at the trailing edge of ramp.
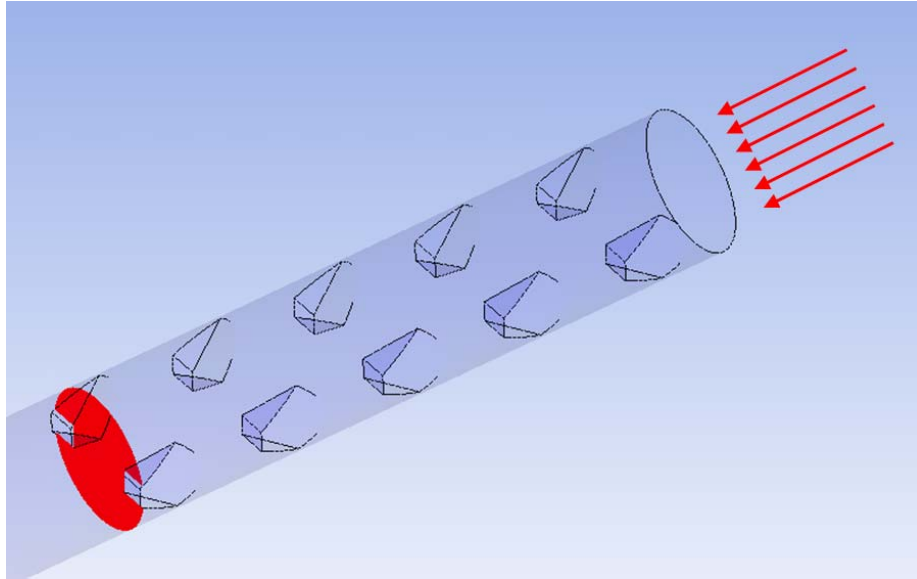
Figure 13.    Illustration of plane of interest for following figures

### 1.    Steady State Analysis of 2R.180.5S Swept Ramp Combustor

The left half of Figure 14 displays the swirling axial flow created by the swept ramp obstacles.  This streamwise vorticity is believed to be a large contributor to the elevated Turbulent Kinetic energies observed in the combustor.  As these rotational structures progress down the combustor, regions of interaction with similar structures create regions of large shear strain rates, and raise the Turbulent Kinetic Energy (TKE) of the flow.  Early comparison of computational models with actual detonation testing has indicated a correlation between TKE values exceeding 200 $m^2/s^2$ and successful DDT for obstacles evaluated in this study.  This correlation may only be valid for three-inch combustors installed in the NPS multicycle PDE utilizing the swept ramps in this study. The maximum velocity achieved in the 2R.180.5S swept ramp simulation was 90 m/s for the inlet Mach 0.2 refresh condition and the Turbulent Kinetic Energy of the flow is approximately 200 $m^2/s^2$.  The high TKEs achieved in this analysis predicted successful DDT in the physical combustor.  It is important to note the overall clockwise global rotation of the rotational structures in Figure 6 as well when viewed from the aft end. These results were used as the baseline to compare other ramp configurations.

21
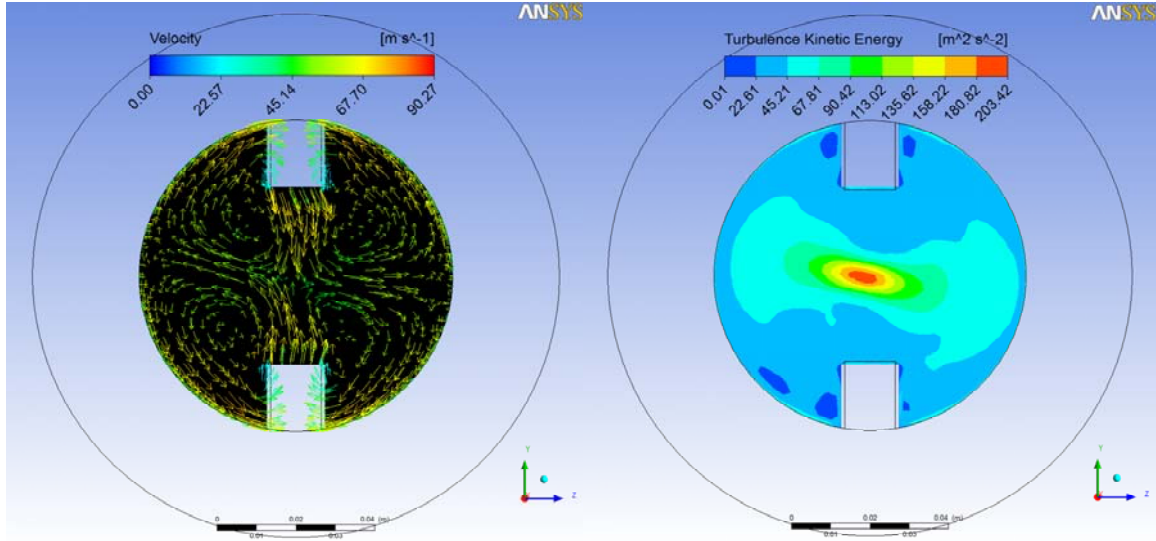
Figure 14.    Cross section view of velocity and TKE in 2R.180.5S swept obstacle field

## 2.    Steady State Analysis of 2R.180.5S Wide Unswept Ramp Combustor

The second portion of the simulations was to determine whether these rotational structures had a significant effect on detonatability.  To analyze these rotational structures appropriately, the unswept ramps were designed maintaining the same height, and associated physical blockage ratio of the swept ramps.  These ramps were placed in the same 2R.180.5S configuration as the swept ramps.  Results for the unswept wide ramps are displayed in Figure 15.  The maximum velocity achieved in this simulation was less than 70 m/s for the Mach 0.2 refresh condition, which is a 30% decrease from the swept ramp model and the associated Turbulent Kinetic Energy of the flow at this plane is just over 40 $m^2/s^2$ at the axial centerline.  There appears to be some local acceleration and vorticity forming at the corner of the ramps, but the core and lateral areas are predominantly axial flow with relatively low values of TKE. Since this geometry fell short of the baseline TKE value of 200 $m^2/s^2$ and upon further review of experimental testing this configuration did not demonstrate the ability to detonate at the nominal test conditions.  This also reveals the detonability of the swept ramp configurations is not merely due to physical blockage, but possibly the fluidic blockage that results from these rotational structures.
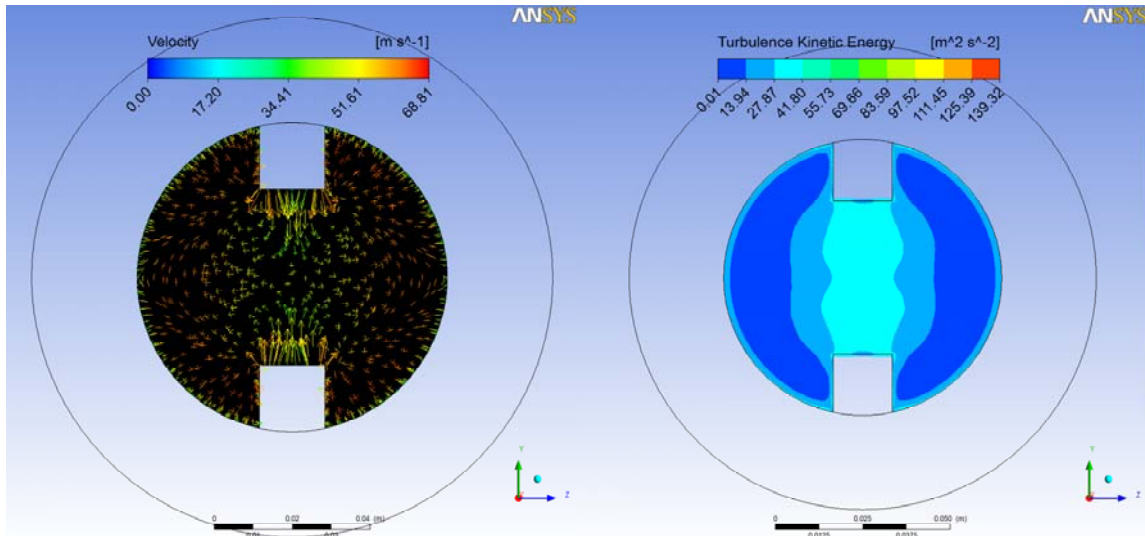
Figure 15.    Cross section view of velocity and TKE in nonswept obstacle field

### 3.    Steady State Analysis of 4R.180.5S Swept Ramp Combustor

For illustrative purposes, a simulation on a combustor with four swept ramps per station was performed.  More vorticity can be observed in the Figure 16 cross sections, and the areas of rotor interaction correspond with regions of high Turbulent Kinetic Energy as observed in the 2R.180.5S swept case.  While the swept ramps are superior for increasing the Turbulent Kinetic energy of the flow field, the point of diminished return appears to be two per station.  The 4R configuration produced 225 $m^2/s^2$ of TKE, but later pressure loss testing revealed its losses to be prohibitive for future use.   The best configuration must not only cause detonation reliably, but do so with minimum pressure loss.
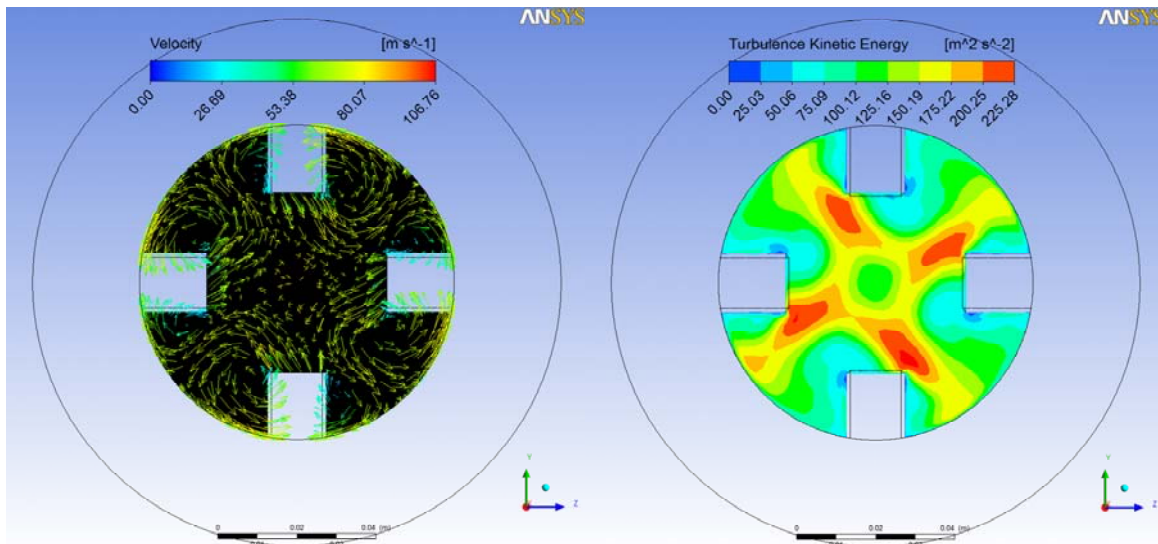
Figure 16.    Cross section view of velocity and TKE in 4R.090.5S obstacle field

# IV.  DESIGN/EXPERIMENTAL SETUP

## A.  PULSE DETONATION ENGINE

This section describes the equipment and techniques used in the experimentation that supports this thesis. All testing associated with this project occurred in the NPS Rocket Laboratory located off campus.  An engine capable of burning both ethylene/air and JP-10/air mixtures was used to complete the desired testing. The NPS Rocket Lab PDE was designed and used for previous experimentation, but the combustor section was altered for the purposes of this work.  Prior to initial testing, The JP-10 fuel injection system was upgraded, but was not used in the conduct these experiments.  The fuel system modification is discussed in the future work section.

The NPS Pulse Detonation Engine is a single tube, "valveless" design that is the culmination of over five years of continuous research by previous graduate students.  The engine consisted of a combustion tube, fuel and air injector systems, and an ignition system.  Each subsystem is discussed in the following paragraphs.  A photograph of the test rig is included as Figure 17.
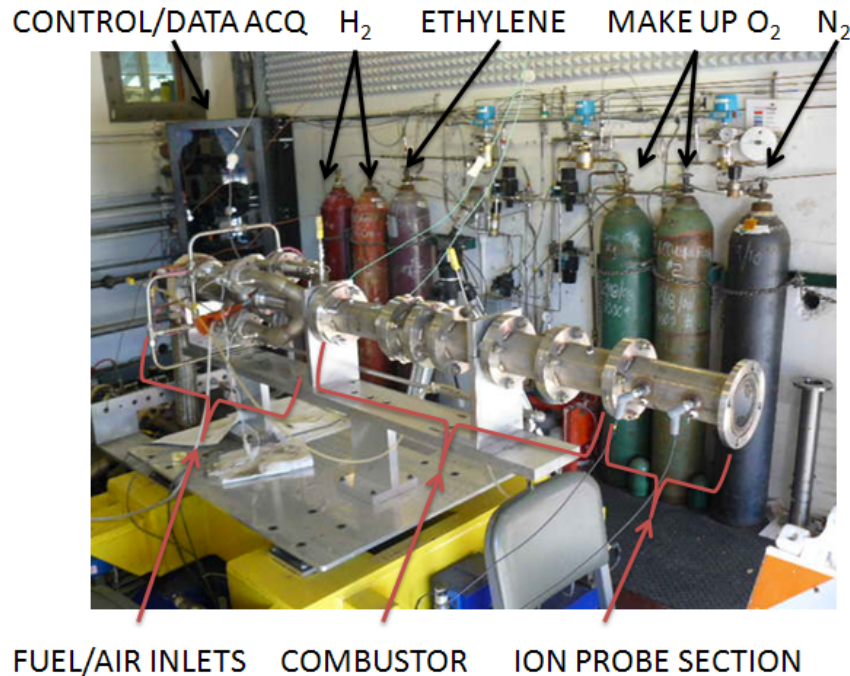
Figure 17.    Photograph of test hardware

### 1.    Air Delivery

The supply air subsystem provided constant flow of vitiated air to the engine at approximately 380K.  Air was delivered from the Hydrogen vitiator (Figure 18) at mass flow rates of up to 0.87 kg/sec (1.92 lb/sec) via a 2" diameter tube.  Following entry of the vitiated air into the engine inlet, it was split into four 1½" diameter fueling arms in which fuel was added.  Choked restriction plates were installed within each of the fueling arms to condition the flow prior to entry into the combustion chamber and isolate the vitiator from downstream pressure oscillations.  This isolation was necessary to prevent combustor pressure transients from affecting the vitiator flame holding. The split flow design provided a more uniform fuel/air injection into the combustion chamber.

In order to simulate flight conditions, air flow into the combustor was heated to approximately 460K.  This was accomplished using the Hydrogen Vitiator pictured in Figure 10.  Hydrogen was injected into the bulk flow at the point labeled Hydrogen supply and ignited by a Hydrogen torch (which uses spark ignition).  Oxygen was added to main air downstream of the vitiator to return the molar fraction to that of atmospheric

air. In practice, the vitiator was operated for 30–45 seconds prior to each test, and ethylene was not introduced until just after the vitiator turned off. This procedure allowed use of the Hydrogen vitiator to heat up all of the surrounding hardware which in turn was able to elevate the temperature of the incoming air sufficiently long after vitiator shut-off. This removed the presence of water and the ambiguity of questionable molar fractions of the reactants delivered to the combustor.
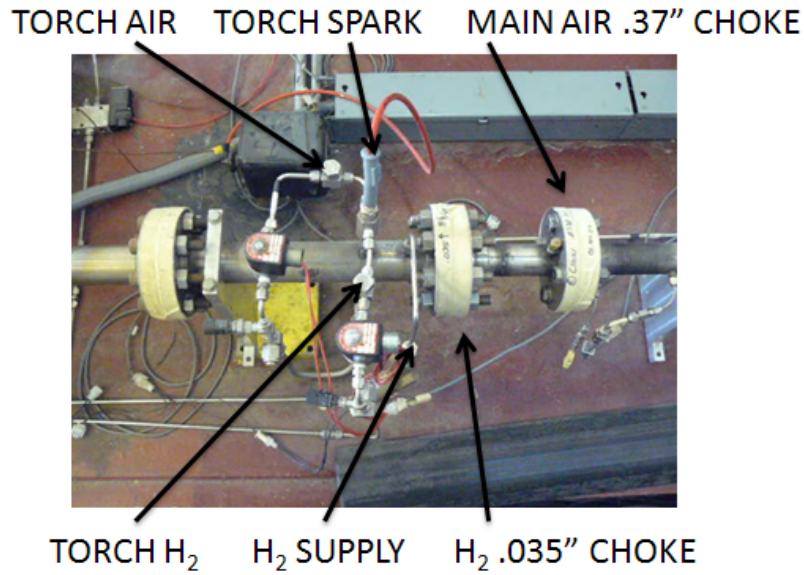


Figure 18.    Cell #2 vitiator setup

### 2.    Fuel Delivery

The fuel injection system was designed to provide control of the stoichiometry of the fuel/air mixture supplied to the combustor. Control of the fuel mixture was achieved by varying the supply pressure of the injected fuel with installed Tescom regulators. Fuel pressure changes altered the mass flow rate ratio of fuel to supply air, which altered the equivalence ratio ($\varphi$). The mathematical expression for equivalence ratio is given by

$$\varphi = [(F/A)/(F/A)_{ST}] \qquad\qquad (10)$$

where (F/A) is the mass ratio of fuel to air for the experimental mixture and $(F/A)_{ST}$ is the mass ratio of fuel to air for the stoichiometric mixture. Performance varied with changing equivalency ($\varphi$) ratio, so accurate measurement and control of fuel injection

was critical. An equivalence ratio near one provides the fuel/air mixture which optimizes both thrust and Specific Impulse ($I_{sp}$). Specific Impulse is the change in momentum per unit of propellant, which is given in Equation 11.

$$I_{SP} = \frac{I_t}{(m_p g_o)} = \frac{F}{(\dot{m} g_o)} \tag{11}$$

An equivalence ratio of $\varphi > 1$ implies more fuel exists than can be combusted with existing oxidizer. This leaves unburned fuel in the combustion products and is called a "rich" mixture. Unburned fuel generally results in lower thrust levels and decreased $I_{sp}$. Conversely, insufficient fuel ($\varphi < 1$) indicates the system required more fuel, which results in less than maximum thrust values, but may yield higher Specific Impulses. As mentioned above, two separate fuel injection systems were installed on this test rig, but only the ethylene system used for this testing is discussed below.

CHOKED RESTRICTOR PLATES     JP-10 FUEL INJECTORS



ETHYLENE INJECTORS     JP-10 INJECTOR COOLING LINES
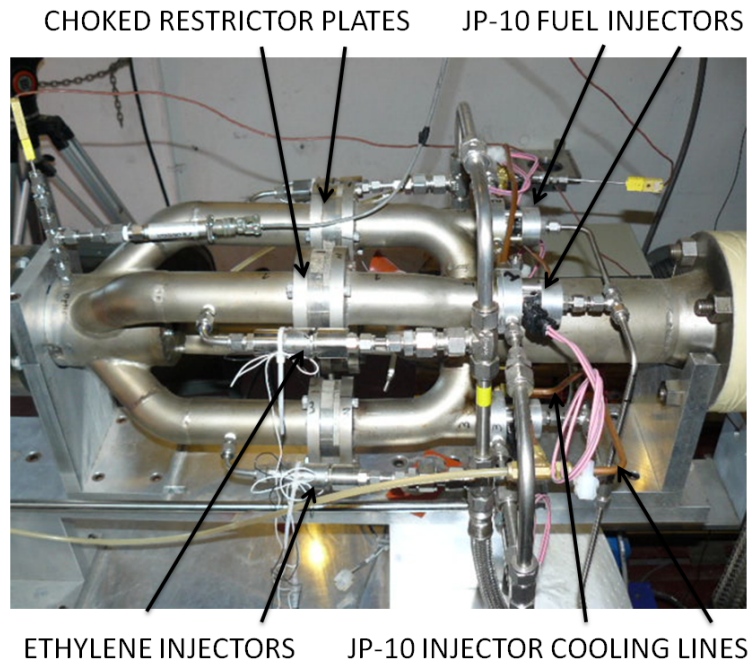
Figure 19.    Picture of fuel arms

A quad fuel injector system was used supply ethylene individually to each of the four fuel arms. Four electrically-controlled high frequency Valvetech (PN#15060-2)

solenoid valve injectors were joined by a common feed manifold and mounted to the fuel arms downstream of the flow chokes. The gaseous fuel mixed with supply air prior to entry into the combustion chamber.

### 3. Ignition System

A team from the University of Southern California, led by Professor Gunderson, designed and constructed a small-scale Transient Plasma Ignition (TPI) system specifically for the NPS PDE. LT Neil Hawkes [22] outlined the advantages of using a TPI system in Pulse Detonation applications. The TPI box (bottom right picture in Figure 20) outputs a high voltage signal to a machined electrode inserted through an orifice directly into the combustion chamber. The TPI signal flowchart is illustrated in Figure 12. A BNC 500 Pulse generator "fires" at the desired operating frequency, which triggers the BNC 575 to produce two output waveforms each time it's triggered. These signal both Trigger and provide a "Rapid Charge" input to the High Voltage Pulse Generator. The final component in the ignition system is the electrode and its housing detailed in lower left photo in Figure 20.
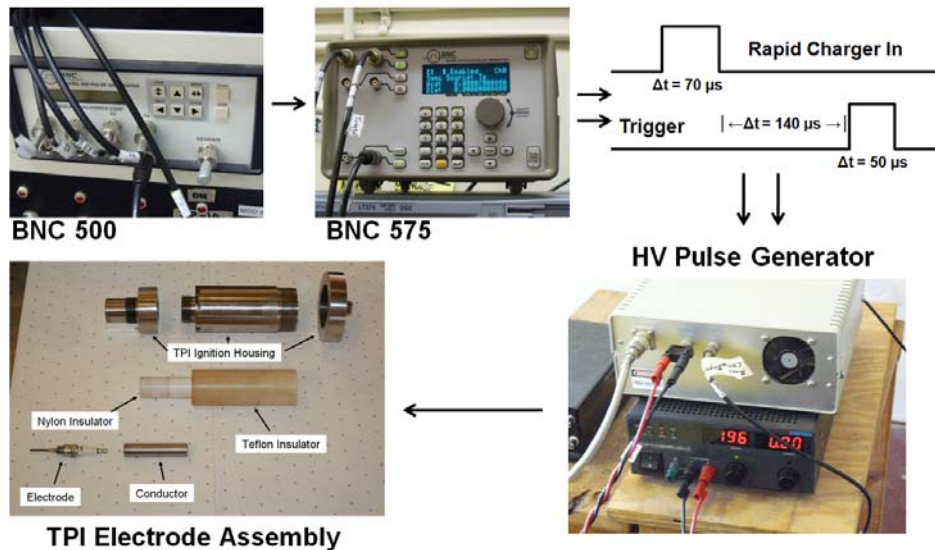


Figure 20.    Signal path for transient plasma ignition

## B.     INSTRUMENTATION

### 1.     Differential Pressure Measurement

Pressure loss measurements were accomplished using a Honeywell FDW differential pressure cell (Figure 21).  The high pressure end was connected via Tygon tubing to the head end of the combustor, while the low pressure end was coupled in similar fashion to the ion probe section downstream of the combustor.  The scale of this detector was 0-10V, and was very appropriate to the magnitude of differential pressures experienced during the testing.  The corresponding output voltages of 0-10.0616V were calibrated using a simple linear correction to accurately indicate pressures in the control software (discussed later).  This system was used to characterize the pressure loss of each combustor configuration under cold flow (no combustion) conditions for Mach refresh numbers ranging from 0.4 down to 0.05.  Curves illustrating the outcome of this testing are displayed in the results section.



Figure 21.     Differential Pressure (DP) cell

### 2.     Ion Probe Wave Front Velocity Measurement

Wave front speeds were measured using an Ion Probe box.  It has 8 separate circuits for measuring combustion wave conductivity.  Each circuit is a simple loop with

a nominal 5V power supply, a motorcycle spark plug gap, and a resistor in series. Output voltage is read across the spark plug gap. When the ion content of the fluid in the spark plug gap is low, the entire 5V is dropped across the gap. When a heavily ionized gas (combustion wave) passes through the gap, the conductivity increases and the corresponding voltage drop decreases. Two circuits were used in the conduct of detonation experiments. One was placed upstream of the other with a four-inch separation. Measuring the elapsed time between voltage drops yields the combustion wave speed. The two spark plugs can be seen at the end of the engine in Figure 17. Figure 22 is a photograph of the box containing the eight separate measurement circuits.



Figure 22.    Ion probe box

### 3.    Thrust Stand

The Thrust Measuring System (TMS) was designed and constructed by Force Measurement Systems of Fullerton, CA. It was capable measuring force in all six degrees of freedom, but testing for this thesis required only axial thrust measurement. The thrust stand has a footprint of approximately 5' x 5', and weighs over 1700 lbs. It is capable of supporting 750 lbs. The thrust range of the stand for the axial force was zero to 500 lbf. The thrust stand is visible beneath the engine in Figure 17, and a close-up of an individual load cell is displayed in Figure 23. Eighteen different load cells coupled the

force from the test bed to the ground.  Of these, 10 were used for data collection and 8 were strictly for calibration.  Each load cell was of shear beam construction, double bridge foil strain gauge, which output changes in strain by varying voltage signals, with full-scale output of 2mV/V. Each load cell was joined with the live bed and ground frame via Universal flexures. Flexures were designed to provide a single point of articulation, prevent free play or hysteresis, and allow for a high degree of accuracy [23].



Figure 23.    Load cell

## C.    SOFTWARE DESCRIPTION AND DATA AQUISITION

The PDE and auxiliary equipment were controlled by a National Instruments Lab View program installed on a personal computer isolated from the test cell in the control room.  The control room PC was linked to a NI PXI-1000B controller in the test cell through an Internet connection to the PXI IP address. The program controlled engine operation by managing gas supply valves located in the test cell and controlling the sequence of events for engine operation.  For safety purposes, the control room contained the 28 VDC and 110 VAC master power switches, and an emergency shutoff button. The electrical switches controlled electrical power within the cell for engine control and instrumentation equipment, such as temperature and pressure transducers. The emergency

shutoff button was capable of disabling the entire test cell by closing all supply gas valves and interrupting fuel injection and ignition trigger signals.

Data acquisition was controlled via the PC in the control room. The PC was linked to the PXI-1000B controller mounted on the wall in the test cell, which in turn was linked to three NI data acquisition devices (DAQ) located on the engine stand. The PXI-6031E was a 16 channel, 16-bit card that collected operational parameters such as various engine temperatures and pressures and supply gas pressures at a rate of 1 kHz. The control program deposited performance and thrust data into an Excel spreadsheet. The LabView Graphical User Interface is shown in Figure 24.
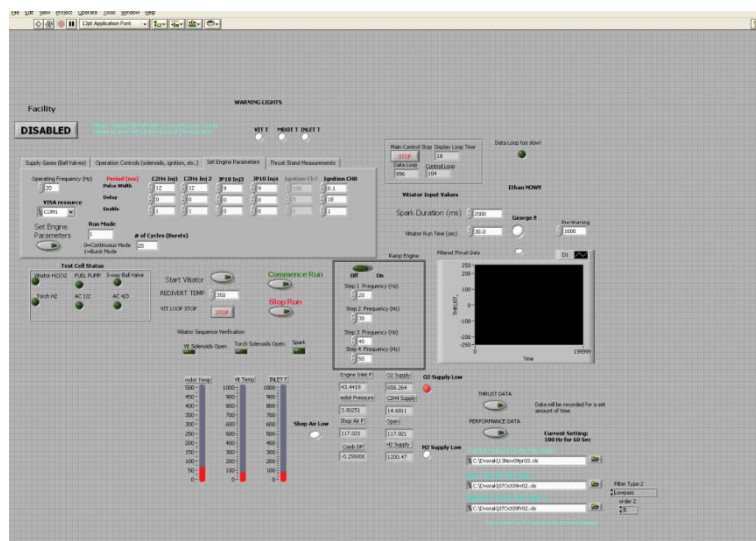


Figure 24.    Lab View VI

THIS PAGE INTENTIONALLY LEFT BLANK

# V.    EXPERIMENTAL RESULTS

## A.    PRESSURE LOSS TESTING

### 1.    Unchoked Combustor Conditions, No Nozzle

The first series of tests evaluated the pressure loss for various ramp obstacle fields.  A complete record of which configurations were pressure tested is shown in Table 4.  The presence of an X in any field indicates that the listed geometry was tested.  No nozzle was used in the conduct of the first tests to allow refresh Mach number to vary freely without experiencing choked conditions at any point.  This allowed all combustor setups to be evaluated at various refresh Mach numbers from 0.05 to 0.4 and with a nominal inlet temperature of 290 K.  Since most practical systems will have to process mass at a practical rates, it is expected that the refresh Mach number for these systems will be in the range of 0.2 to 0.3.  Several ramp configurations were abandoned early on due to poor performance during previous tests.
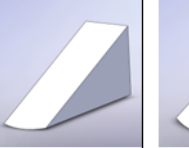


| CONFIG | SWEPT TALL | SWEPT SHORT | POINTED | UNSWEPT | UNSWEPT WIDE |
|---|---|---|---|---|---|
| MAX BR | 13.1% | 8.32% | 10.47% | 9.96% | 13.1% |
| 2R.180.4S | X | | | X | X |
| 2R.180.5S | X | X | X | | X |
| 2R.180.6S | X | | | X | X |
| 2R.180.8S | X | | X | | |
| 1R.360.6S | X | | | | |
| 1R.360.8S | X | | | X | |
| 3R.120.4S | X | | | | |
| 3R.120.6S | X | | | | |
| 4R.090.4S | X | | | | |
| SPIRAL.4S | X | | | | |
| SPIRAL.8S | X | | | | |
| INTER.4S | X | | | | |
| INTER.5S | X | | | | |

Table 4.    Tabulated test matrix (no nozzle).  X indicates configuration tested.

The below results are compared to a Shchelkin-like spiral, which is a very conventional transition device used in previous detonability studies [24].  Figure 25 displays pressure loss data for all tests, while Figure 26 illustrates only the results pertinent to this discussion.  There is a noticeable increase in the total pressure loss of the

spiral over that for the 6 and 5 station tall ramp fields, as shown in Figure 26. The difference is approximately 27% at a refresh Mach number of 0.2, and over 60% at a refresh Mach number of 0.3 between the spiral and 6-ramp combustor. Due to the exponential nature of the curves, the improvement tends to increase as the Mach refresh number increases. Legends for Figures 25, 27, and 29, and 30 are included in Appendix D.
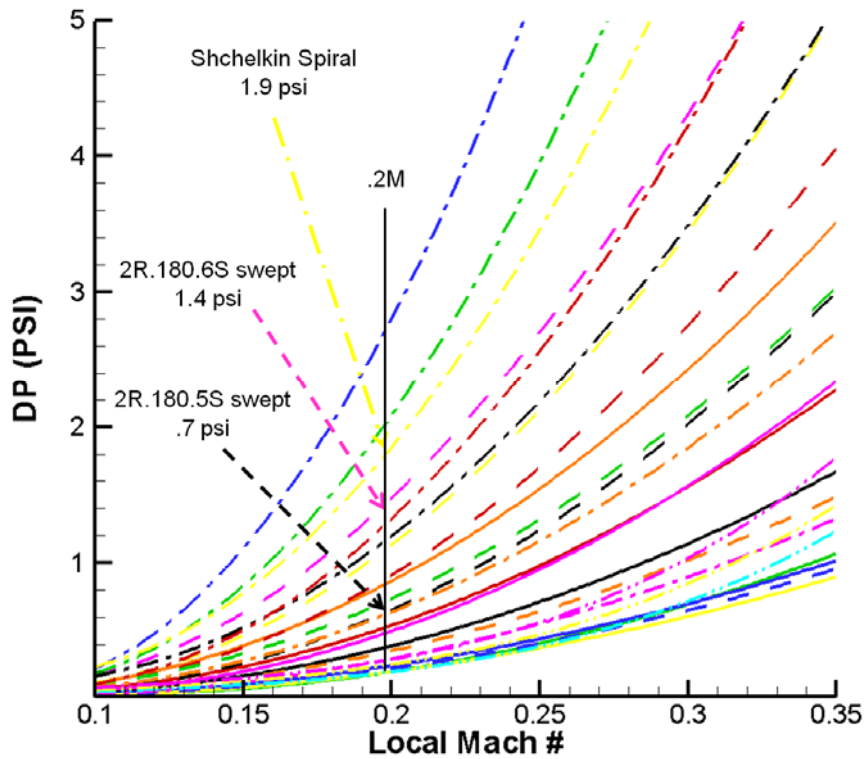


Figure 25.    Differential Pressure loss vs. local Mach number
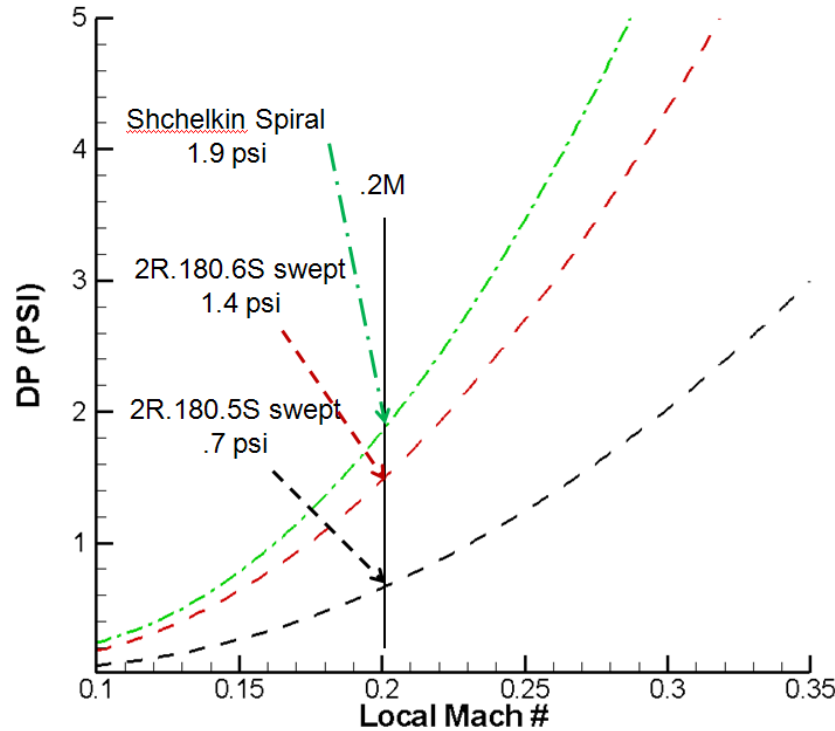
Figure 26.    DP loss vs. local Mach number

Figure 27 displays Percent Pressure Drop $(\Delta P/P_3)$[1] as a function of local Machnumber for all unchoked cases.   Figure 28 highlights the data for previously discussed three cases.  Percent pressure loss is better metric for quantifying performance of the combustor due its widespread use in industry.  An early goal of this research was to identify combustors that have less than 5% pressure loss in the vicinity of Mach 0.2. Historical losses for comparable RAMJET systems have been on the order of 5-10%. Satisfying lower pressure loss requirements is a key element in assuring a place for PDE's in the propulsion realm.  Additional attention was paid to the configurations within the box that also facilitate successful DDT.

---

[1] $\Delta P$ is the pressure drop across the combustor and $P_3$ is the inlet pressure.
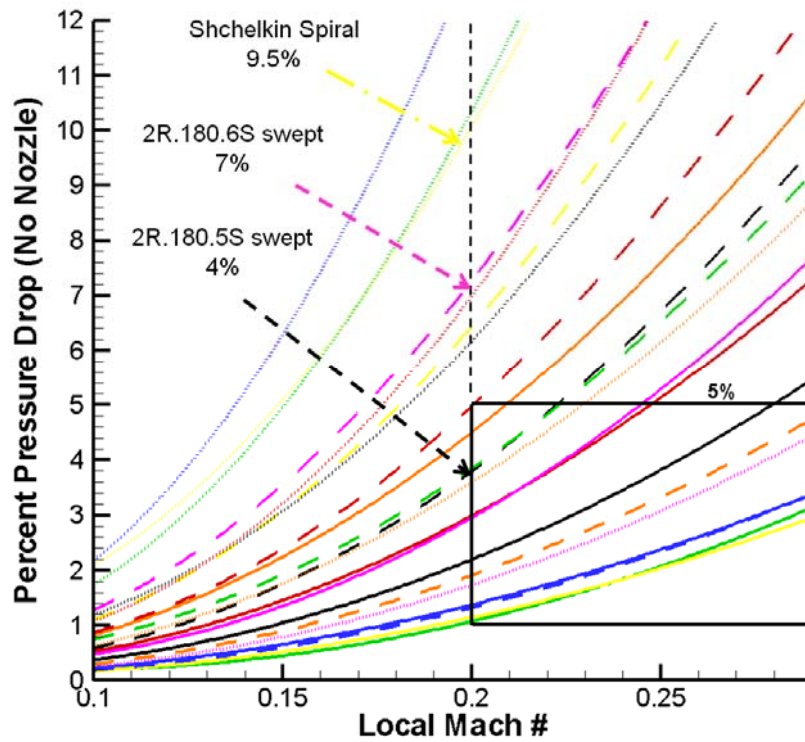
Figure 27.  Percent pressure loss vs. local Mach number
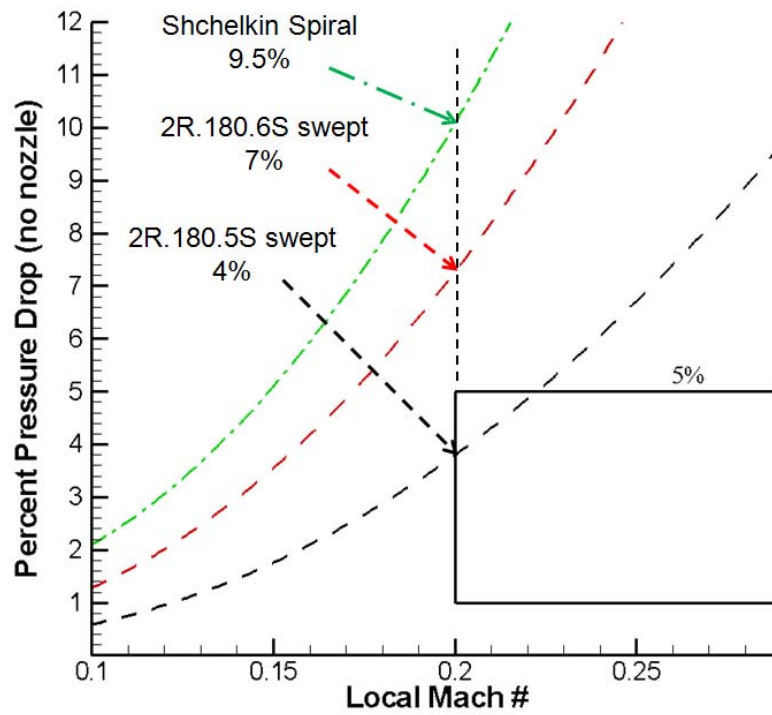


Figure 28.  Percent pressure loss vs. local Mach number

## 2. Choked Conditions

Since practical systems will require the use of a nozzle for performance, similar pressure loss tests were performed with a nozzle which produced a 0.2 Mach refresh condition in the combustor. The nozzle was designed for 0.2 Mach, but boundary layer "pinching" of the flow field yielded choked conditions at around a Mach number of 0.185. The increased fuel mass flow rates necessary were rarely achievable practically, as it required "topped off" tanks to ensure proper fuel mass flow rate for the Valvetech solenoid valves. Table 5 illustrates the minimal extent of choked pressure loss testing.



| CONFIG | SWEPT TALL | SWEPT SHORT | POINTED | UNSWEPT | UNSWEPT WIDE |
|---|---|---|---|---|---|
| MAX BR | 13.1% | 8.32% | 10.47% | 9.96% | 13.1% |
| 2R.180.4S | X | | | X | X |
| 2R.180.5S | X | X | | | X |
| 2R.180.6S | X | | | | X |
| 2R.180.8S | X | | | | |
| 1R.360.6S | X | | | | |
| 1R.360.8S | X | | | | |
| 3R.120.4S | X | | | | |
| 3R.120.6S | X | | | | |
| 4R.090.4S | X | | | | |
| SPIRAL.4S | X | | | | |
| SPIRAL.8S | X | | | | |
| INTER.4S | | | | | |
| INTER.5S | X | | | | |

Table 5.    Tabulated test matrix (0.2M nozzle)

Representing pressure loss as a function of local Mach number for choked-nozzle cases was not very informative since the independent axis never exceeds the choked value. While the plot in Figure 29 is not interesting from a research standpoint, it served to validate the nozzle design. The raw data points do not exceed (in general) a combustor Mach number of 0.185 due to exit nozzle contraction ratio.
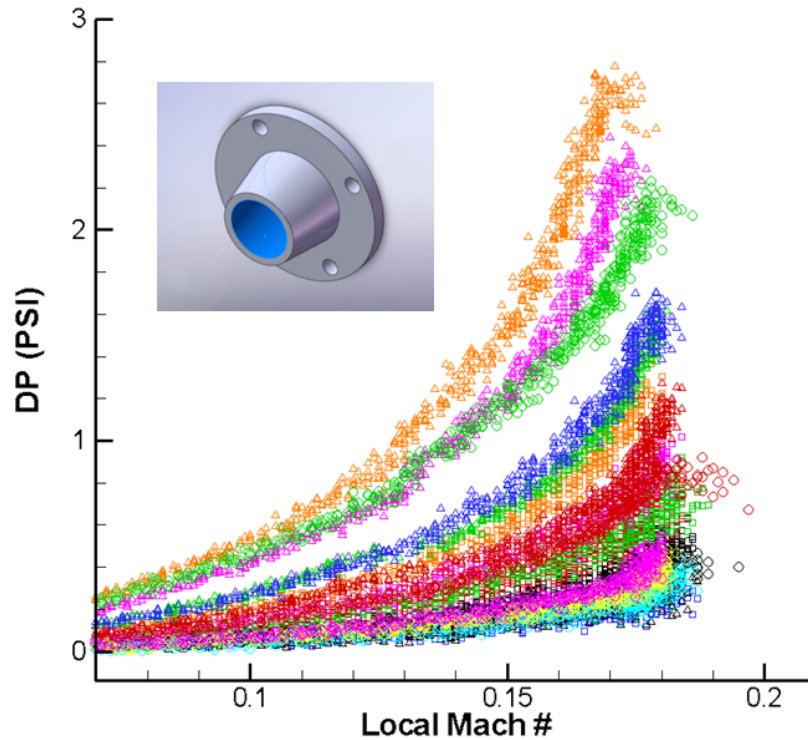
Figure 29.    Differential Pressure vs. local Mach number (0.2M nozzle)

A plot of the normalized Percent Pressure Drop as a function of Reynolds number is presented in Figure 30.    Again, a plot containing combustors germane to this discussion are shown in Figure 31.  The diagonal black line approximates the point along each plot that choked conditions are achieved.  The data for the Shchelkin-like spiral did not quite fit a second order curve, so the curve fit was manually corrected the upper portion and left the data points on to display fidelity.  Of specific interest are geometries that result in less than a 5% pressure drop, which both the 5 and 6 station swept ramp combustors accomplished easily.   The spiral combustor results in approximately 6% pressure loss while the swept ramp configuration loses just over half of that (3.2%) under choked conditions.

40
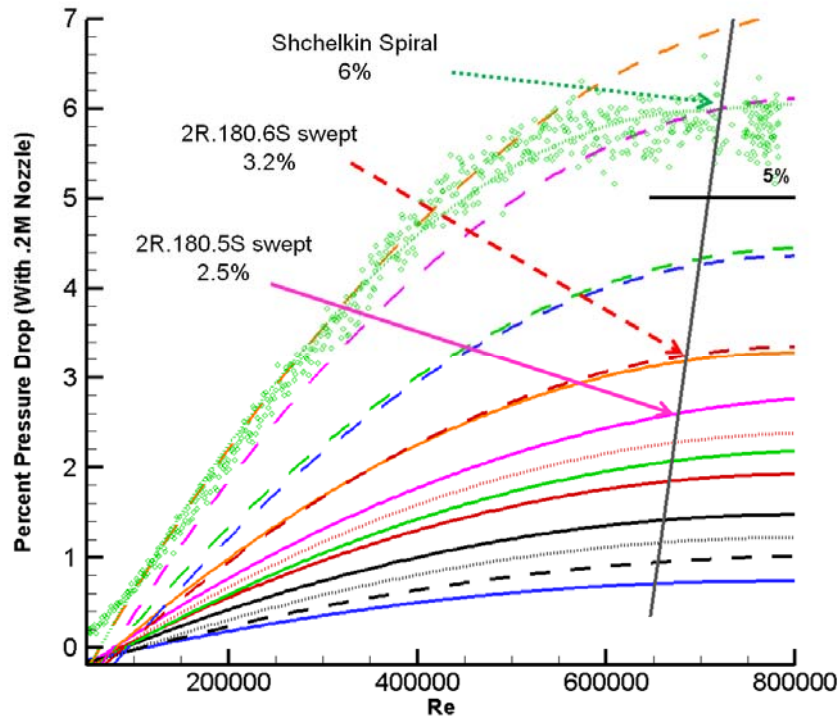
Figure 30.    Percent pressure loss vs. Reynolds number (0.2M nozzle)
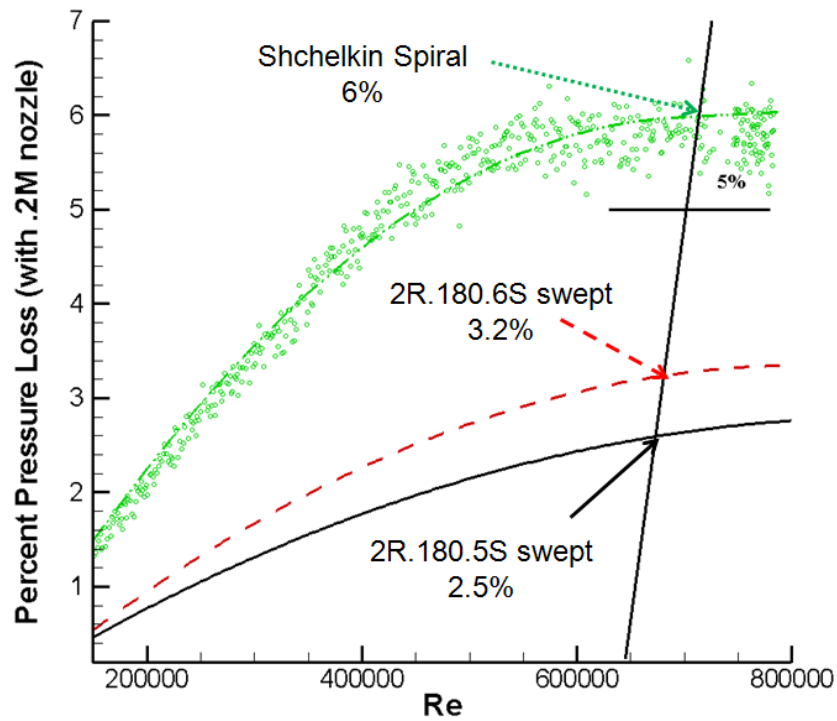


Figure 31.    Percent pressure loss vs. Reynolds number (0.2M nozzle)

## B. DETONATION TESTING

Although the total pressure loss improvements were encouraging, the functionality of each configuration still needed to be verified. Detonability tests were performed at stoichiometric equivalence ratios for all configurations indicated in Figure 35. Red highlighting indicates no detonations, green is for strong, consistent detonations, and yellow indicates marginal detonability. Detonability was measured using Ion Probes as described in the experimental setup section.

Figure 32 displays the ion probe traces for the spiral combustor case. The time difference between the flame front passages between the two ion probes after the obstacle field was approximately 50 μsec. A distance of 0.1016m between the two probes corresponds to a wave front speed of 2032m/sec. A similar calculation using the 60 μsec Δt of the 2R.180.6S in Figure 33 yields a wave front speed of 1693 m/sec. These both exceed the threshold of 1,500 m/sec, above which we are confident a detonation existed, vice transient weak detonations which can easily degrade into subsonic combustion.
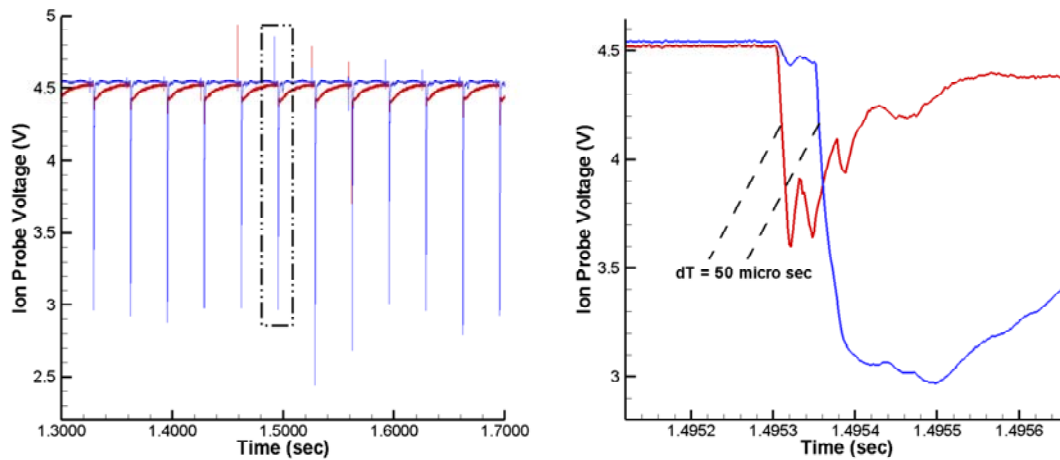


Figure 32.    Ion probe traces for Shchelkin spiral combustor (right figure is boxed region)
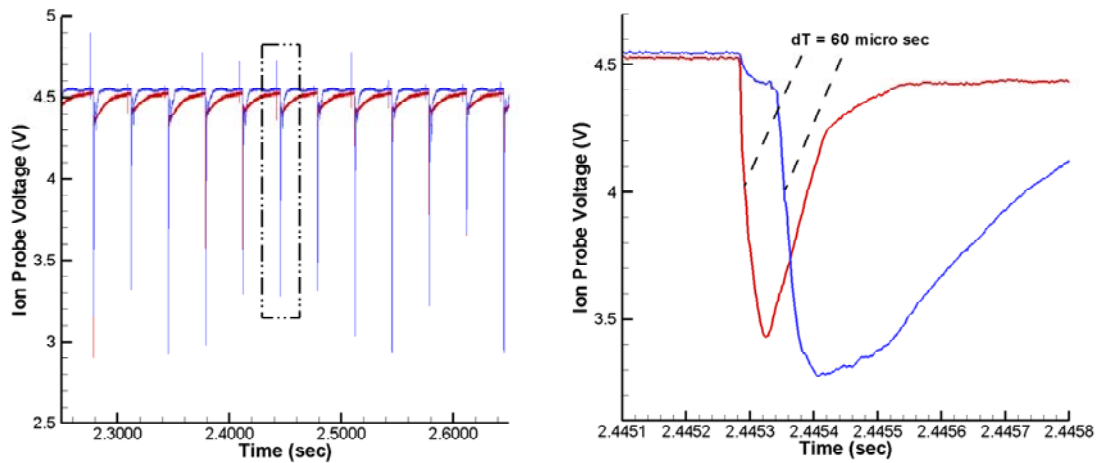
Figure 33.    Ion probe traces of swept 2R.180.6S combustor (right figure is boxed region)

Figure 34 highlights the inability of the non-swept ramps to cause detonations. The flame front leading trace (red) never causes sufficient ionization to increase conductivity in the ion probe gap by any appreciable amount, and the subsequent trace (blue) illustrates the relatively slow subsonic velocities that this event achieved.
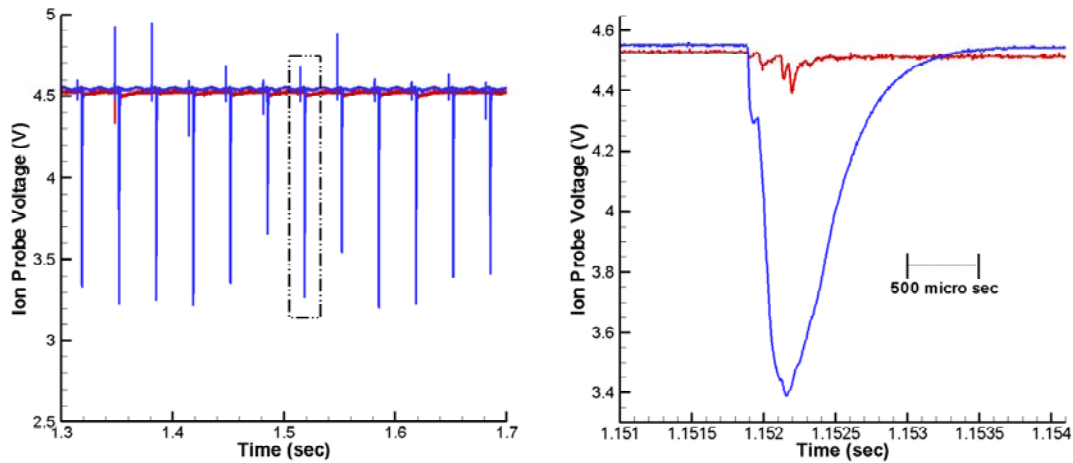


Figure 34.    Ion probe traces of un-swept 2R.180.6S combustor (right figure is boxed region)

Detonation testing for the nozzleless cases appeared to validate earlier CFD results.  The unswept wide ramps were unsuccessful as predicted, and the 2R.180.5S tall-swept case was marginal.  This reinforces the use of TKE and Shear Strain rate as predictors for minimum DDT configurations.  Since the 5 Ramp combustor fell just short

of consistent detonations, we concentrated on the 6 station setups as these represented the shortest physical length for consistent DDT as highlighted in Figure 35.  Of these, only the swept tall ramps were successful.  Testing was largely confined to unchoked conditions due to air and fuel mass flow rate constraints.  The tabulated data indicates that higher combustor pressures (smaller cell size and increased reaction rates) provided by the nozzle decrease the number of required stations by one or two.

**With .2 Mach Nozzle**

| CONFIG | SWEPT TALL | SWEPT SHORT | POINTED | UNSWEPT | UNSWEPT WIDE* |
|---|---|---|---|---|---|
| MAX BR | 13.1% | 8.32% | 10.47% | 9.96% | 13.1% |
| 2R.180.4S | X | | | X | X |
| 2R.180.5S | X | X | | | X |
| 2R.180.6S | X | | | | X |
| 2R.180.8S | X | | | | |
| 1R.360.6S | X | | | | |
| 1R.360.8S | X | | | | |
| 3R.120.4S | X | | | | |
| 3R.120.6S | X | | | | |
| 4R.090.4S | X | | | | |
| SPIRAL.4S | X | | | | |
| SPIRAL.8S | X | | | | |
| INTER.4S | | | | | |
| INTER.5S | X | | | | |
| INTER.6S | | | | | |

**No Nozzle**

| CONFIG | SWEPT TALL | SWEPT SHORT* | POINTED* | UNSWEPT | UNSWEPT WIDE |
|---|---|---|---|---|---|
| MAX BR | 13.1% | 8.32% | 10.47% | 9.96% | 13.1% |
| 2R.180.4S | X | | | X | X |
| 2R.180.5S | X | X | X | | X |
| 2R.180.6S | X | | | X | X |
| 2R.180.8S | X | | X | | |
| 1R.360.6S | X | | | | |
| 1R.360.8S | X | | | X | |
| 3R.120.4S | X | | | | |
| 3R.120.6S | X | | | | |
| 4R.090.4S | X | | | | |
| SPIRAL.4S | X | | | | |
| SPIRAL.8S | X | | | | |

6S represents shortest physical length for consistent detonations with no nozzle

Figure 35.    Summary of detonation testing (Ethylene/Air $\phi$=1.0)

The original "tall" swept ramp configuration is an extension of previous thesis work in a single pulse combustor, but the subsequent four geometries were designed with an eye toward isolating the flow conditions most conducive to Detonation to Deflagration Transition (DDT).  The "short" swept ramp concept was intended to initiate the same reliable DDT as the tall version, but with lower pressure loss.  As shown above, the configuration was unsuccessful.  The pointed ramps were created with similar intention. The idea was to maintain the stream wise vorticity that the swept ramps introduce to the flow field (same height and length of swept side), but with lower pressure loss.  This

setup was more successful than the short swept ramps, but still failed to achieve the benchmark success that the original swept geometry enjoys. The unswept ramps were an attempt to determine the dominant flow field patterns associated with proper DDT. In CFD studies of the flow field, we determined that the unswept ramp introduces little stream wise vorticity. In fact, it predominately yields recirculation perpendicular to the combustor axis which could ultimately result in flameholding. This setup also failed to yield detonations with any consistency. The final iteration of the unswept ramp had the same blockage ratio in order to truly isolate the turbulent mechanism responsible. The "wide" unswept configuration was unsuccessful as well, indicating that physical blockage ratio was not directly responsible for the DDT behavior observed. Drawings of each ramp geometry are included in the attached Appendix C.

## C.    THRUST TESTING

Measuring the thrust output of our non steady-state pulse detonation engine presented several engineering obstacles. The first is the oscillatory nature of its thrust output. To compensate for this, the raw thrust data was passed through a 4 Hz low pass filter, which effectively removed any oscillating thrusts and left only the underlying "DC" bias of the data [24]. This "DC" portion of the data was the gross thrust of the engine. All thrust output plots shown in this thesis were filtered in this manner.
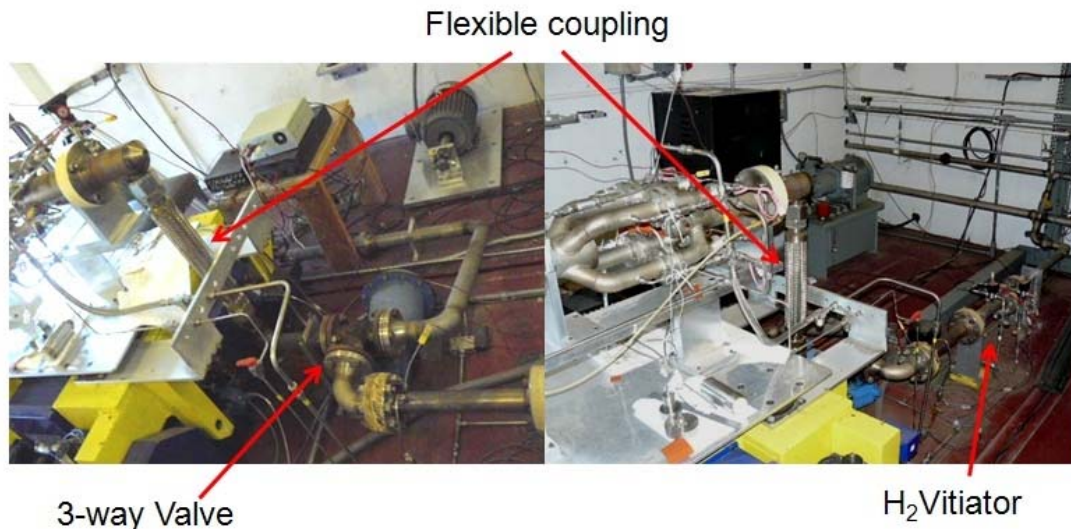


Figure 36.    Flexible coupling

Complicating matters further was the thermal expansion of the non symmetrical flexible coupling (Figure 36) that connected the vitiator/air supply plumbing to the engine inlet. The thermal expansion had significant effects on the output thrust measurement. Figure 37 displays the gross thrust of the engine with only vitiated air flowing (no combustion). As the coupling was pressurized and expanded, it caused significant and increasing negative thrust until the vitiator timed out at approximately 29 seconds. As the coupling cools and contracts, the tare force decreased until the three-way ball valve diverted air around the combustor. The complete unloading of the tare force when the three-way valve repositions suggested that the pressurization "stiffening" of the coupling also played a significant role.
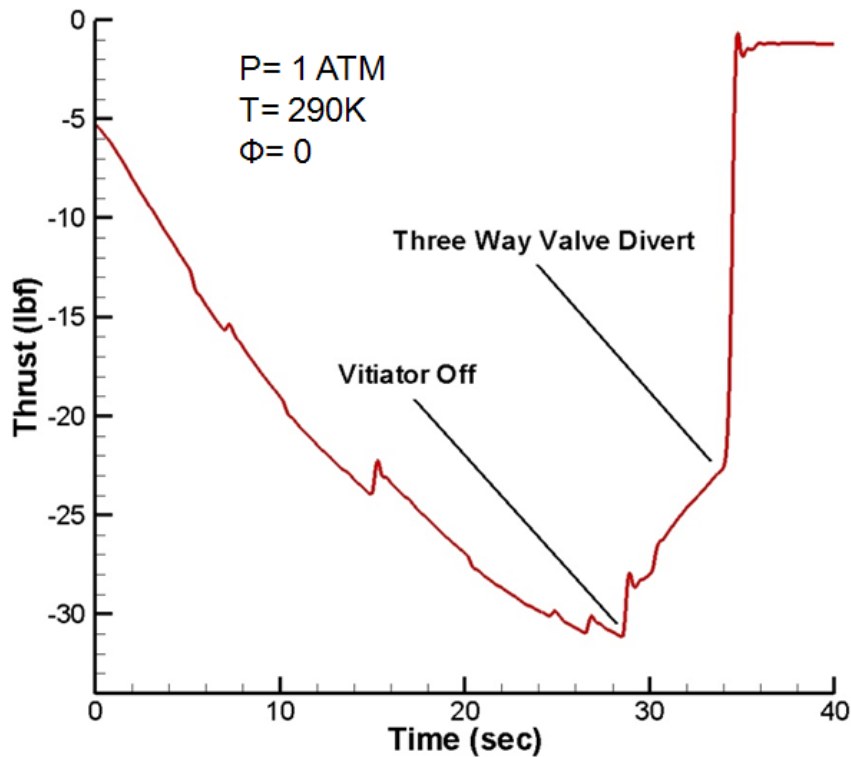


Figure 37.   Measurement of thermal expansion "bias" thrust acting on stand

To compensate for these disturbance forces, the difference in thrust between the instant prior to engine shut-off and just after engine shut-off was measured. Another way to look at this technique is to consider what thrust "went away" when the engine cut off.

The logic backing this approach is the fact that the coupling temperature is comparable immediately following any given combustion test. The three-way ball valve does not divert for roughly 5–10 seconds following a test, so stiffening of the coupling for each test is comparable. Results for the baseline spiral and six station "tall ramp" configurations are displayed in Figures 38 and 39.

The benefits of reduced total pressure losses discussed earlier are also directly visible when thrust values are measured for both configurations. Figures 38 and 39 show the resulting thrust values when the same conditions are detonated by two different combustor configurations. The thrust values presented are simply engine-on and engine-off type conditions and should not be viewed as a net thrust term. They are presented for comparison purposes only. The thrust performance with the spiral is shown in red and is noticeably lower than the levels for configuration with eight of the swept-ramp obstacle stations with two ramps per station. The improvement of the swept ramp combustor (25 lbf) over the spiral configuration (18 lbf) is similar to the reduction in pressure loss between the two setups (27%). This suggests that any savings in pressure across the combustor translates proportionally to an increase in thrust.
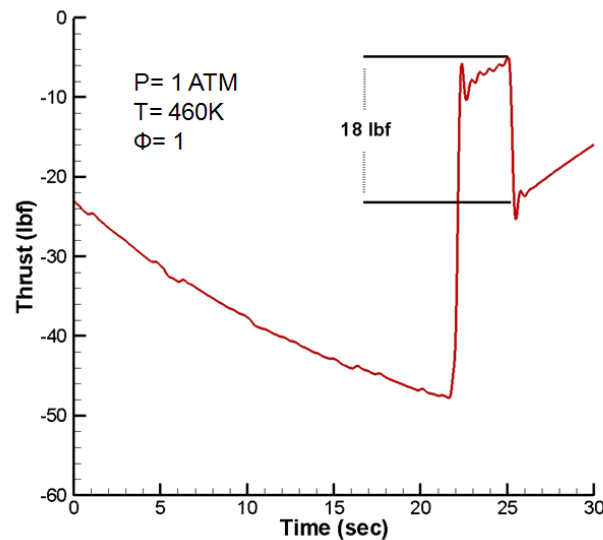


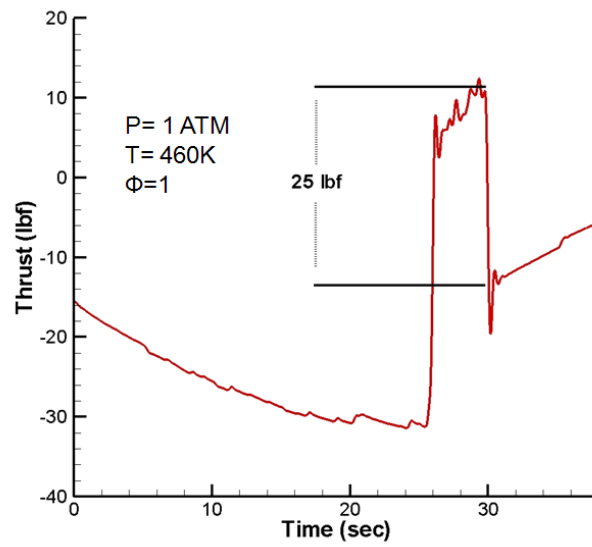Figure 38.    Thrust test of Shchelkin spiral combustor at 30 Hz with vitiator off

Figure 39.    Thrust test of 2R.180.6S combustor at 30 Hz with vitiator off

# VI. CONCLUSIONS

The ability to reliably and efficiently detonate hydrocarbon/air mixtures is a mandatory requirement for practical PDE system development. A large portion of previous (and current) PDE systems operating at modest frequencies often employed the use of Shchelkin-like wall spirals to achieve detonation initiation in a reasonable distance and time. The inherent penalty with wall spiral approaches is the total pressure losses incurred throughout the engine cycle, which results in lower net thrust values. Additionally, the longevity of spiral obstacles is questionable due to the requirement for active cooling. The utilization of swept-ramp obstacles for deflagration-to-detonation transition purposes in PDE systems has significant system performance implications such as very low total pressure loss, attractive thermal management characteristics, and effective initiation over short distances when a fully developed flame condition exists at the entrance to the obstacle field. The flame/vortex interaction, associated small-scale turbulence production mechanisms, and subsequent explosion phenomena are believed to be the primary reason for the favorable DDT performance. Although constant axial spacing of the swept-ramp field was maintained, it appears as though proper "tuning" of the ramp field and post-ramp explosions could effectively shorten the overall DDT distances.

The total pressure loss for the swept-ramp obstacle configuration evaluated has been shown to be at least a 27% improvement over the total pressure loss of a wall spiral with the same DDT performance. This improvement has been directly observed in thrust measurements and can result in more available thrust for the same test conditions as a wall spiral device. Additionally, the thermal management of these devices appears to be much more favorable than the wall spiral configurations, due to the method of installation in the system and increased contact area with the combustor wall. The dynamic nature of PDE systems and the gas dynamics associated with cycle-to-cycle operation make it difficult to probe the detailed mechanisms at work for these devices, but the current results clearly show favorable performance characteristics, and follow-on work is

continuing in an attempt to provide a more detailed understanding of the swept-ramp dynamics and generate guidelines for how swept-ramp obstacle fields may impact future engine designs.

# VII. FUTURE WORK

## A. INCREASING THE SCALE AND COMPLEXITY OF THE TEST RIG

Very rarely does any technology reach its full potential. Automobile engineers continue to revise and rethink the reciprocating engine over one hundred years after its invention. Pulse detonation Combustors are in their infancy, but incremental progress is leading to unique designs with bigger scale and greater practicality. This section summarizes the continued efforts of those working at the NPS Rocket Propulsion Lab in the area of Pulse Detonation technology. Several improvements outlined in this chapter were completed during the course of this project.

The current single tube test rig has reached its limit as a proof of concept device. The next stage of development is a three tube test engine with thrust vectoring capability. One criticism of PDEs is the non-steady thrust they provide, while drag is always present. Thrust Vectoring allows a tactical missile to guide itself without external control surfaces, which reduces drag. A conceptual drawing of the new design is displayed in Figure 40. This design necessitates increased fuel and air flow in addition to cooling capability to allow longer test runs.
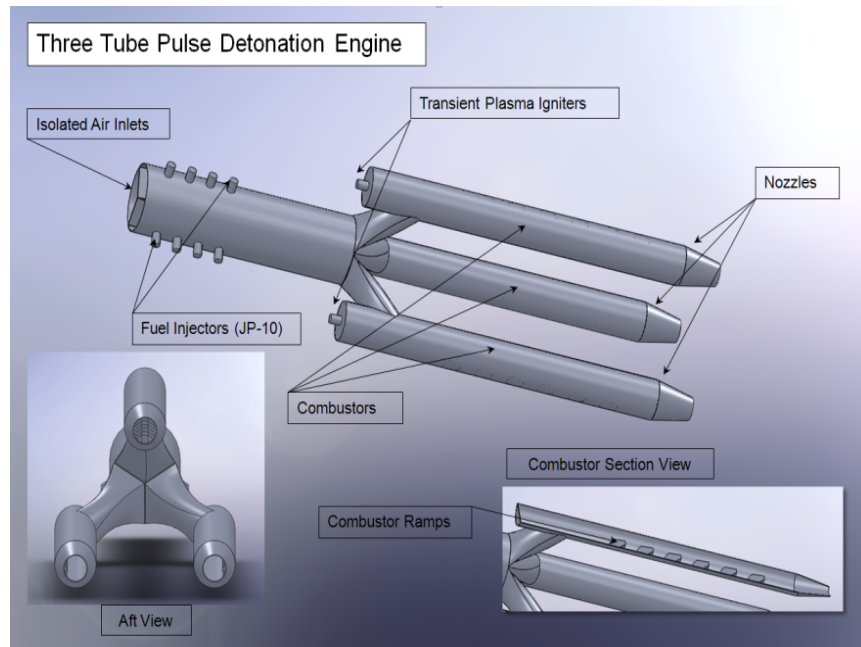
Figure 40.     Conceptual drawing of three tube PDE

## B.     COMBUSTOR COOLING JACKET DESIGN

Thermal analysis is being performed to design a cooling jacket for each combustor in the three tube test engine.  In six-second test runs, the single combustor rig reached peak temperatures in excess of 500ºF (Figure 41).    While the observed temperatures are not extreme, the rapid increase limits testing to six second runs.  Initial designs of the cooling system will focus on single-pass water cooling, but the eventual goal is to cool the combustor with JP-10 before injection and eventual ignition.  Not only will this cool the engine and allow longer test runs, but it will preheat the fuel and increase performance.
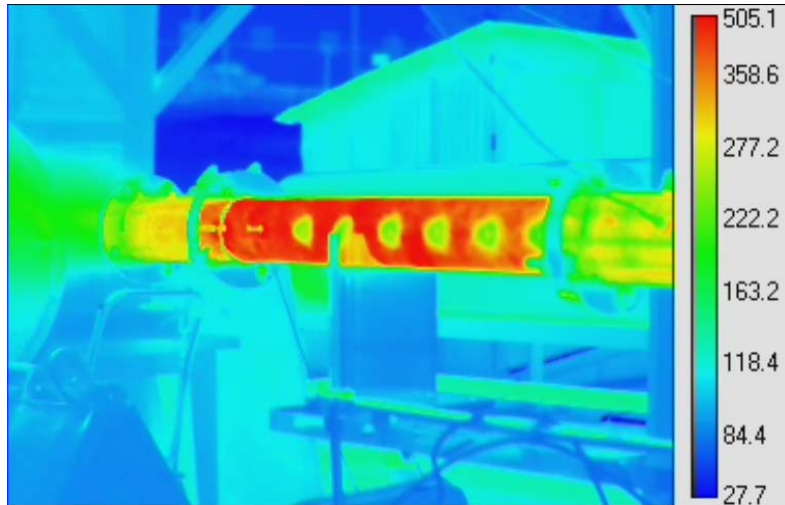
Figure 41.    Thermal imaging of six-second test run at 30Hz

## C.    INCREASE FUEL AND AIR FLOW TO THE COMBUSTOR

A three tube engine operating under choked conditions will require a substantially increased mass flow rate of air and fuel.  Three large cylinders were recently installed (Figure 42), which increased the high pressure air capacity by approximately five times.



Figure 42.    Air farm at NPS rocket propulsion lab

Pictured below in Figure 43 is a newly installed JP-10 fuel injection pump. This pump is fed by a nitrogen pressurized flask that supplies JP-10 at approximately 50 psi. The pump is capable of delivering 2900 psi, but will have an output recirculation line that regulates the pressure felt by the installed Bosch fuel injectors.



Figure 43.    JP-10 injection pump

## D.    REPLACE VITIATOR

The currently installed Hydrogen vitiator is troublesome in several respects. First, the use of Hydrogen and make-up oxygen ($O_2$) calls the chemistry of air provided to the combustor into question. For this reason, the vitiator is used only to warm the test rig and associated piping to temperatures necessary simulate flight conditions. This introduces a second problem: the thermal expansion during warm up and subsequent contraction after vitiator cut off severely biases the thrust output data. For this reason, a new shell and tube heat exchanger is scheduled for installation. The new system is capable of heating the increased air throughput to flight conditions while maintaining a physical boundary between the heating fluid and incoming combustor air. Installed hardware will be similar to the heat exchangers shown in Figure 44.
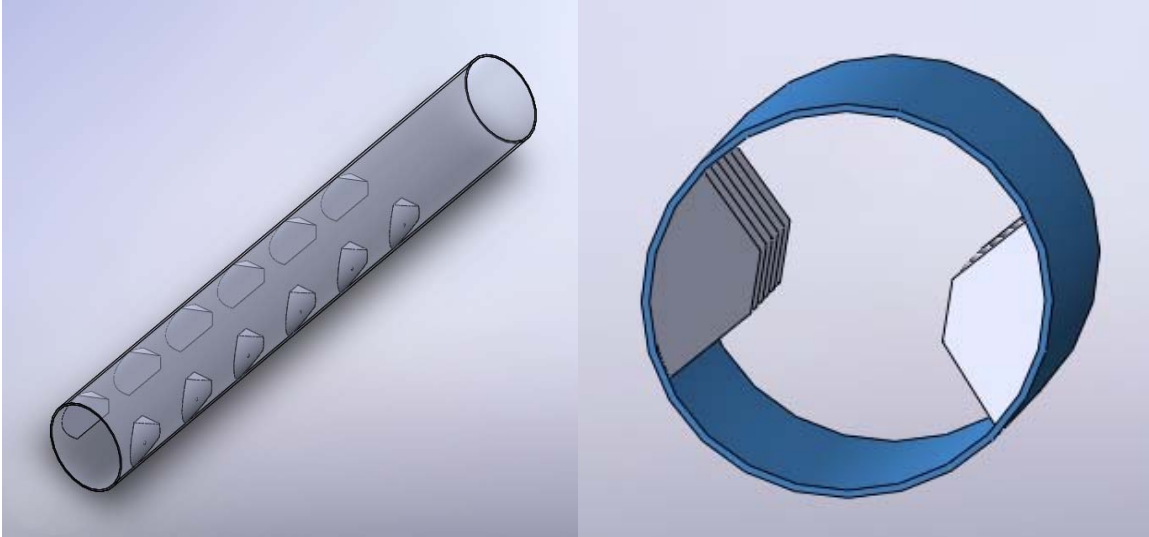
Figure 44.    Shell and tube heat exchangers

THIS PAGE INTENTIONALLY LEFT BLANK
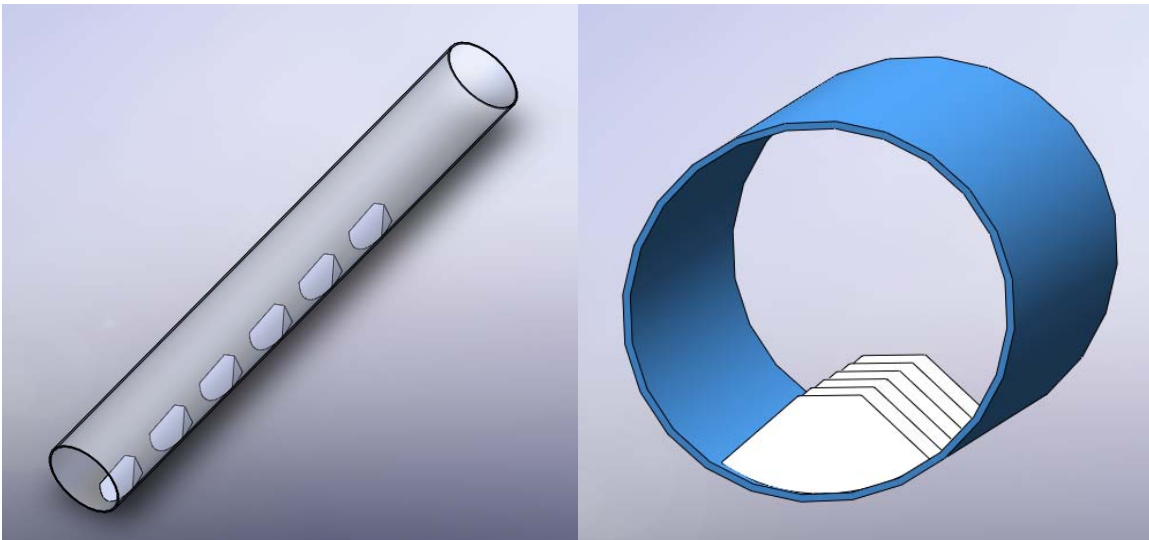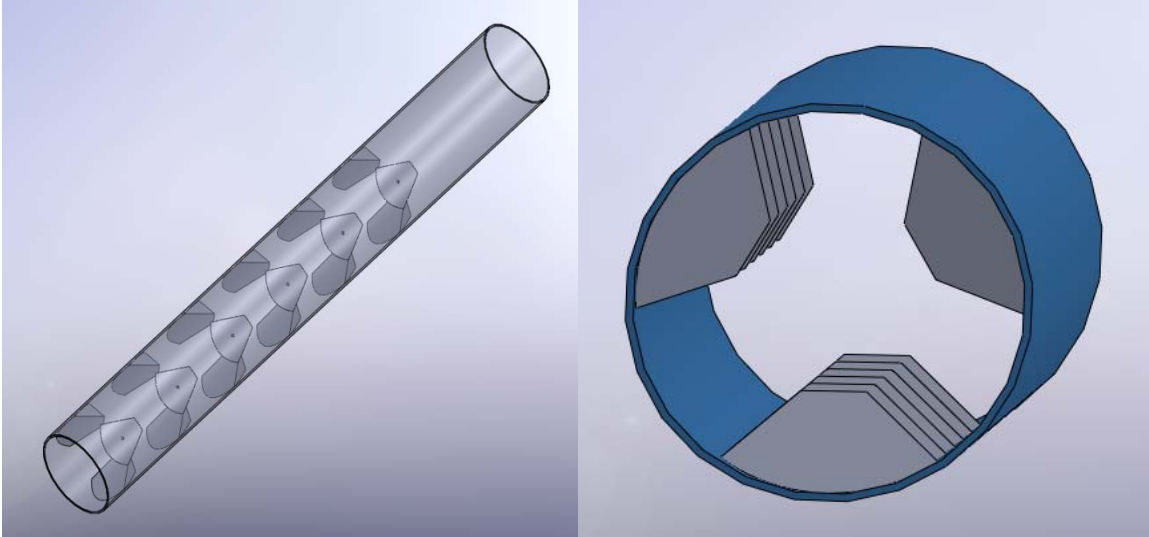
# APPENDIX A:  CONFIGURATION EXAMPLES

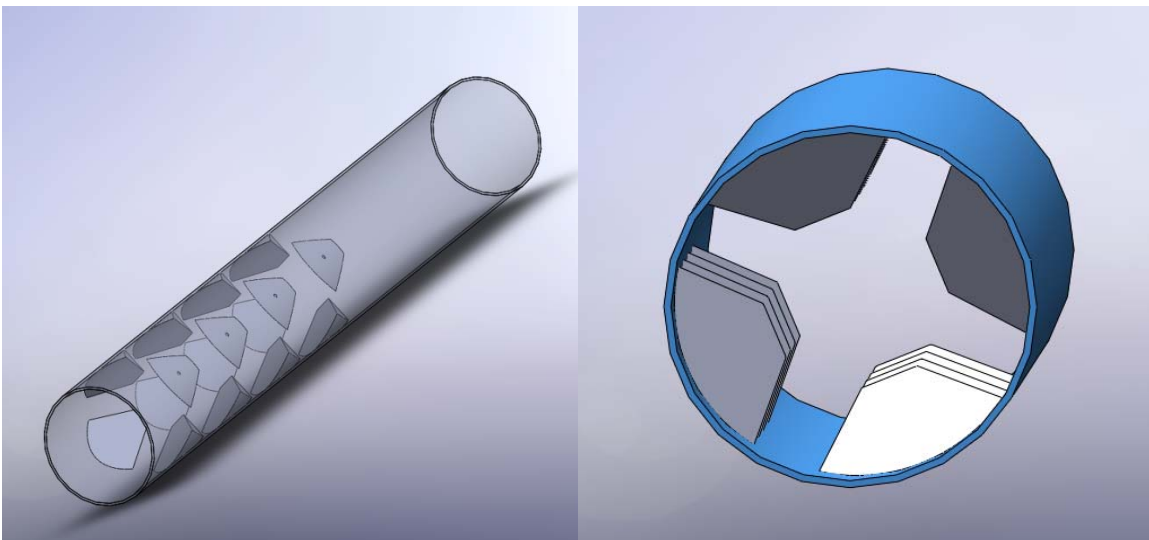**A.**     **2R.180.4S**
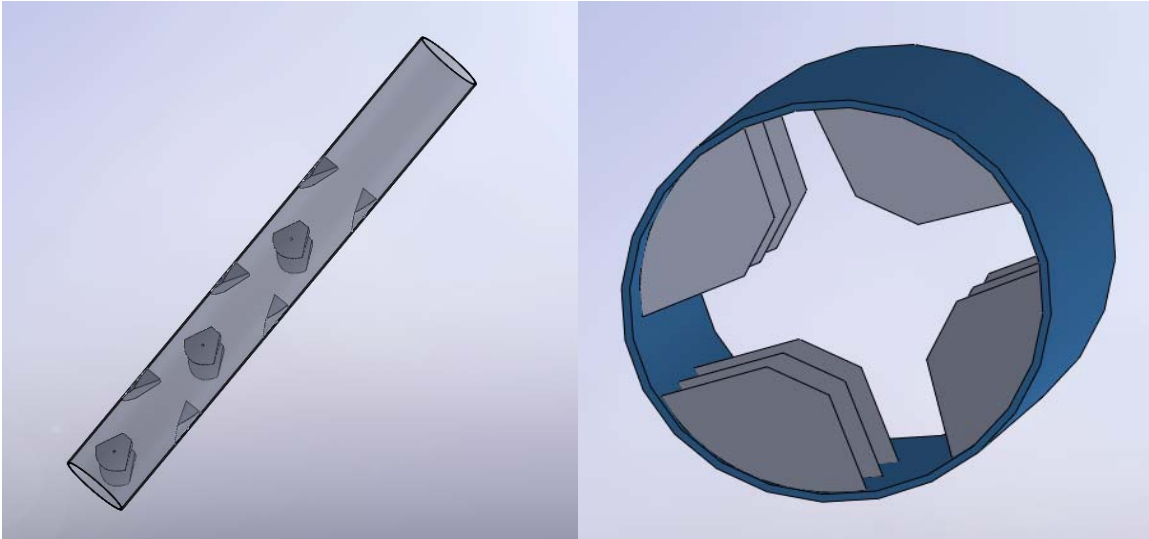


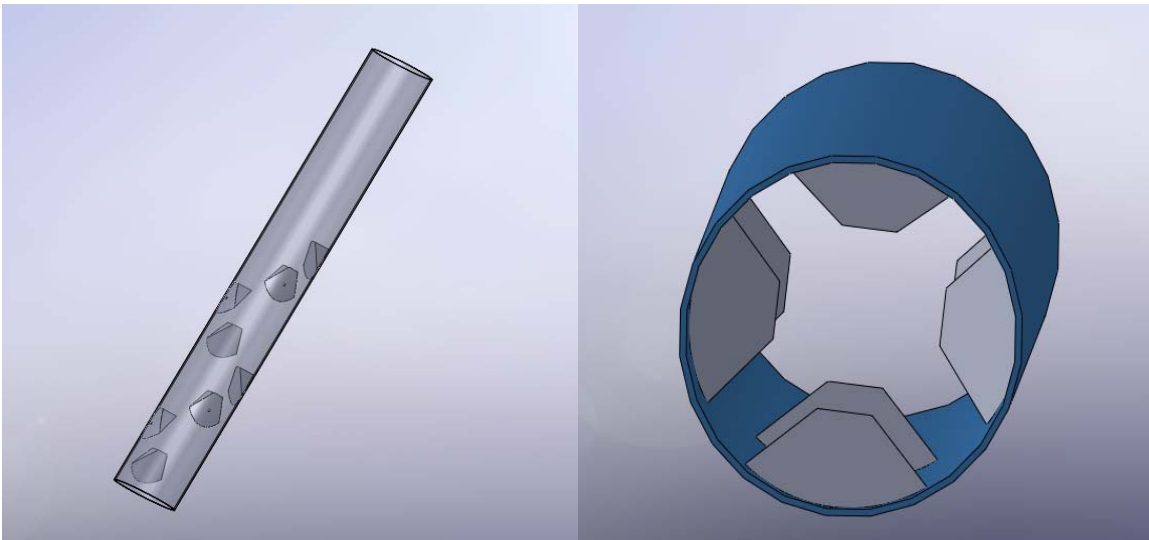**B.**     **1R.360.6S**

**C.     3R.120.6S**



**D.     4R.090.4S**

**E.      INTERDIGITATED.6S**



**F.      SPIRAL.8S**

THIS PAGE INTENTIONALLY LEFT BLANK

# APPENDIX B:  PULSE DETONATION ENGINE SOP

Test Cell #2
Standard Operating Procedures (S.O.P)
**Engine Start UP**
**(last modification date 15 Oct 2009)**

**Prior to starting preparations**
1. Notify all lab personnel of live test cell.
2. Turn ON control console
3. Turn ON warning lights
4. Notify the Golf Course (x2167) (Only required if Hot Fire Test is conducted)

**Preparing Test Cell**
1. Push the Emergency Stop IN (secured)
2. Turn ON BNC Cabinet Power Strip.
3. On Control Computer, open LABVIEW and ensure that the execution target contains the PXI address. Open control panel and run the program.
   a. RT Target address: 172.20.120.118
   b. Control Program Path
      i. Open
      ii. Test Cell #2 Manual Control v20 (runs v19b)
      iii. Enter Run Path Name
              1. If this is not completed prior to running you will lose the data file that was created with the default name.
4. Turn ON 24 VDC in the control room cabinet
5. OPEN Main Air (HP Air Tank Valve) and High Pressure Air
   a. Blue hand valve should be opened slowly as not to shock the lines
   b. Node 4 air valve in test cell #1 open
6. OPEN $H_2$ & $O_2$ six packs
7. Enter Test Cell #2 and OPEN all the supply gas bottles that are going to be used
8. OPEN both JP-10 valves
9. Ensure that PXI Controllers, Kistlers, and Power strip in the black cabinet are ON.
10. Turn ON 24 VDC power supply for Test Cell #2 TESCOM Control Power.
11. OPEN Shop Air, Isolation Valve (High Pressure Air) and Main Air
12. If JP-10
    a. CLOSE 440 VAC knife switch for Oil Pump (ON)
13. TURN ON Cooling Water (If required)
14. TURN ON TPI (do not exceed 85 on heater control knob) – 30-60-85 (1 min intervals)
15. CONNECT Vitiator Spark Plug.
16. If required, set up any visual data recording equipment.
17. Evacuate all non-essential personnel to the control room
18. Check Shop Air Compressor in heater room– approx 120 psi min

19. RUN the control
20. Close Blast Door
21. Lock Gate

**Running the Engine**
1. Set Main Air, Secondary/Purge Air, and all other gases pressures (ER3000) ON RPL00
    a. Set Main Air and Purge Air (ER3000)
        i. 01 Main Air
        ii. 04 Secondary Air – Set to 220
    b. Supply Gases in Test Cell #2 TESCOM Node Address
        i. 20 Vitiator $H_2O$
        ii. 21 Vitiator $O_2$
        iii. 22 $C_2H_4$
2. **DISCONNECT CH 7 & 8**
3. Set All Engine Control Parameters (on BNC Pulse Generator)
    a. Send Engine Parameters to BNC
4. **RECONNECT CH 7 & 8**
5. Twist Emergency Stop Button clockwise (TEST CELL IS NOW LIVE)
6. ENABLE the Test Cell on the VI.
7. OPEN Vitiator, Torch, and $C_2H_4$ Ball Valves.
8. Verify Golf Course is clear
9. SOUND the Siren
10. START recording on VCRs
11. Fuel Pump On (If using JP-10)
12. TURN ON Data Recording Switch
13. Manually engage Main Air flow
14. START Vitiator

*****************************WARNING**********************************
The next step will result in the commencement of a run profile and ignition.
* Note: The 3-Way Ball Valve has a control in the Vitiator sequence. If the Vitiator is used then the 3-Way Ball will not divert through the engine until 375º F and will dump overboard at the end of the run at 175º F.
15. COMMENCE RUN
    a. High Speed DAQ will be triggered and the engine profile will commence
16. STOP RUN.
    a. Pulse generation will be stopped.
17. TURN OFF Data Recording Switch
18. Wait for main air to divert
19. STOP Main Air Flow
20. Ensure all Ball Valves are closed
21. Fuel pump OFF (If using JP-10)
22. DISABLE the Test Cell on the VI.
23. Push Emergency Stop Button IN

Test Cell #2
Standard Operating Procedures (S.O.P)
**Engine Shut DOWN**
**(last modification date 15 Oct 2009)**

1. SET all supply gases to ZERO, Nodes 1, 4, 20, 21 & 22
2. CLOSE all gas supply valves using LabView
3. STOP control code.
4. Push Emergency Stop Button IN
5. Turn OFF Power Strip in BNC Timing Cabinet
6. If Gas Turbine Igniter (Test Cell #1) used DISABLE BEFORE turning off 24 VDC
7. TURN OFF 24 VDC power supply (check with other test cells first)
8. CLOSE Jamesbury Valve (check with other test cells first)
9. REMOVE Vitiator Spark Plug head
10. SECURE TESCOM 24VDC power. (check with other test cells first)
11. CLOSE Shop Air, High Pressure Air, and Main Air
12. If using JP-10
    a. OPEN 440 VAC Knife switch (OFF)
13. TURN OFF Cooling Water
14. CLOSE Supply gases
15. CLOSE JP-10 supply valves
16. TURN OFF TPI
17. CLOSE $H_2$ & $O_2$ six packs
18. VENT $H_2$ & $O_2$ lines
19. STOW Cameras and other equipment used in testing.
20. CLOSE Test Cell #2.
21. TURN OFF Warning Lights.

THIS PAGE INTENTIONALLY LEFT BLANK

# APPENDIX C: COMPONENT DRAWINGS
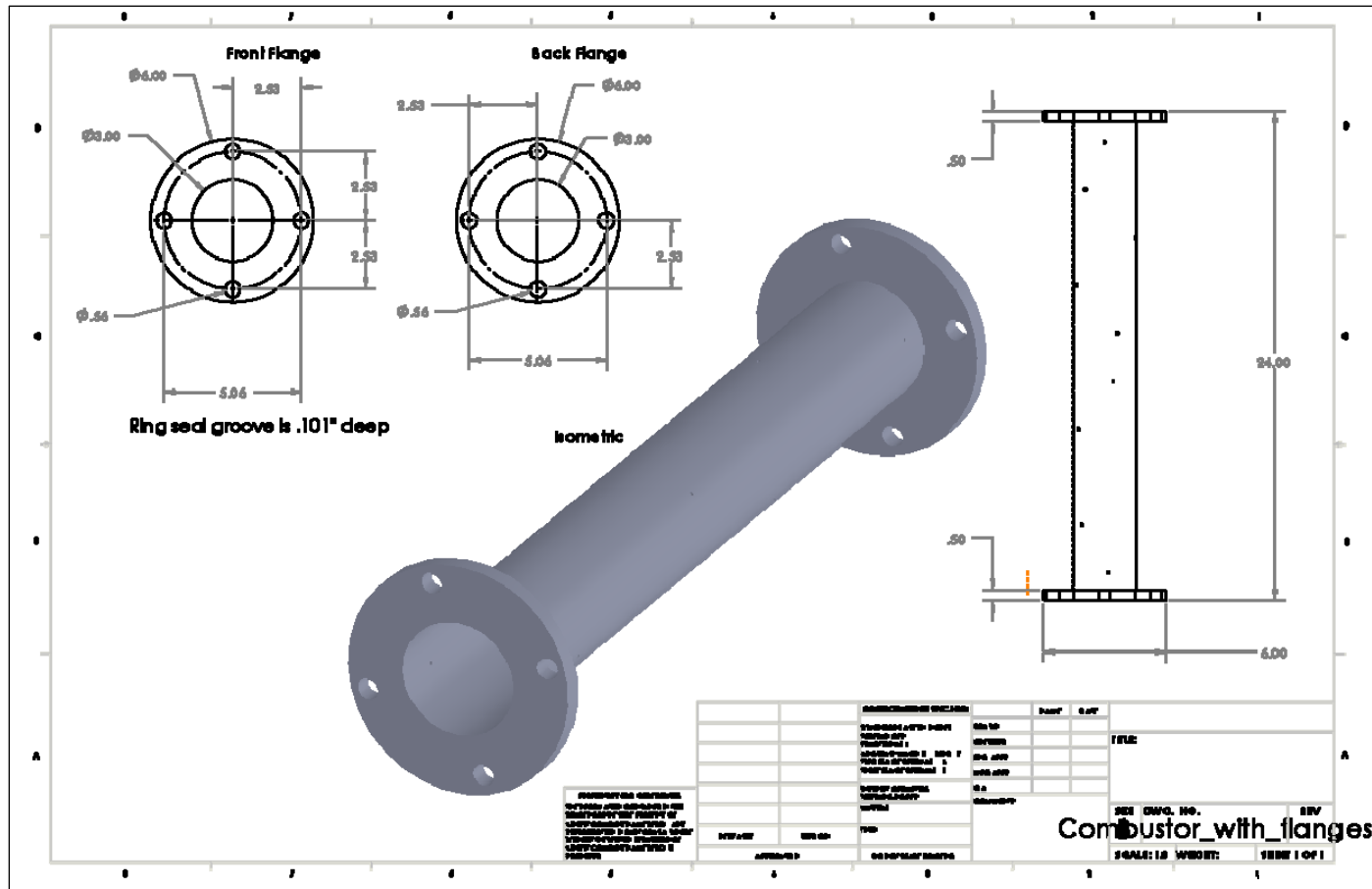


Figure 45.    Combustor drawing
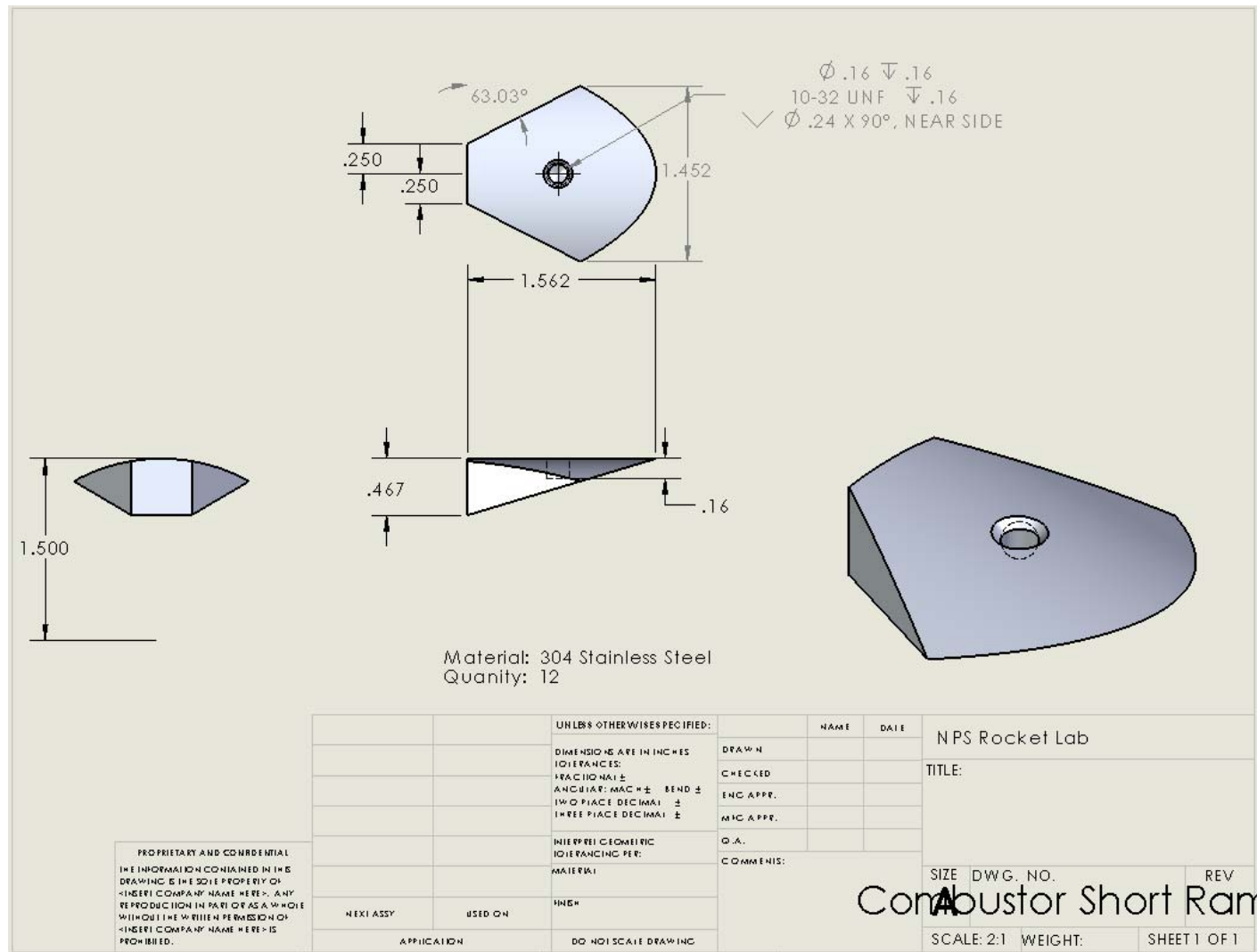
Figure 46.　0.2 Mach nozzle

66

Figure 47.    Tall swept
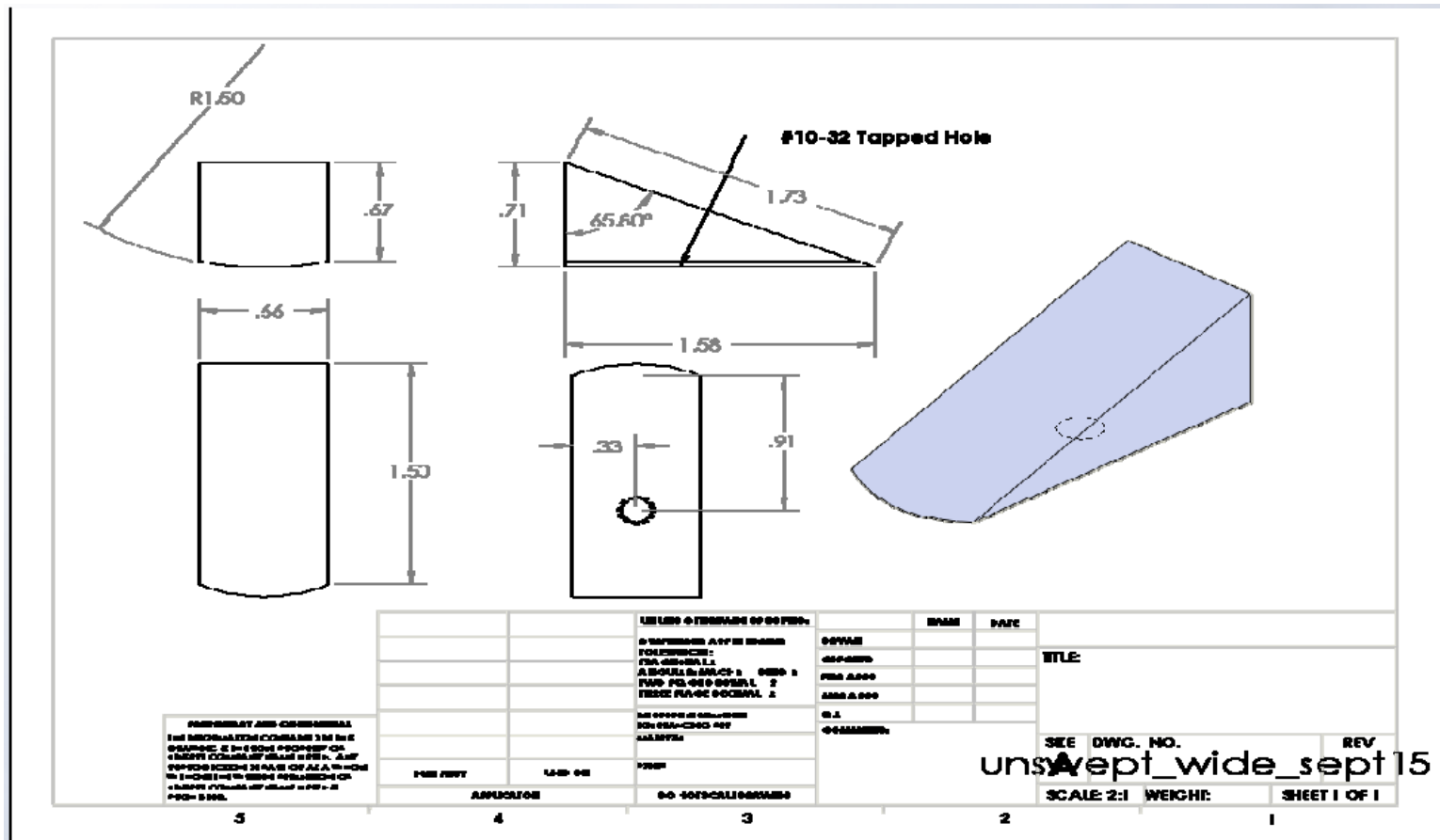
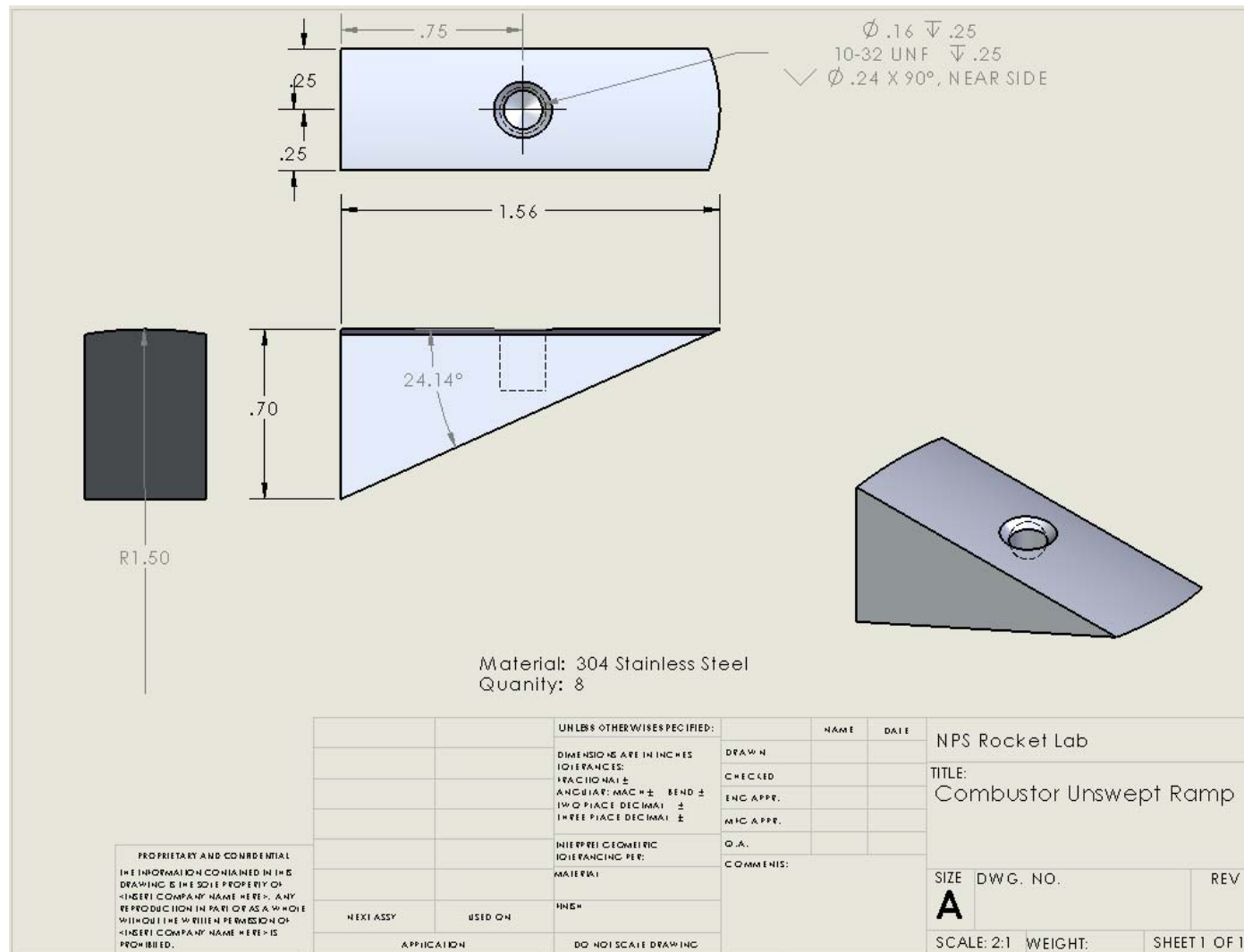Figure 48.    Short swept

68

Figure 49.    Wide unswept

69

Figure 50.    Unswept
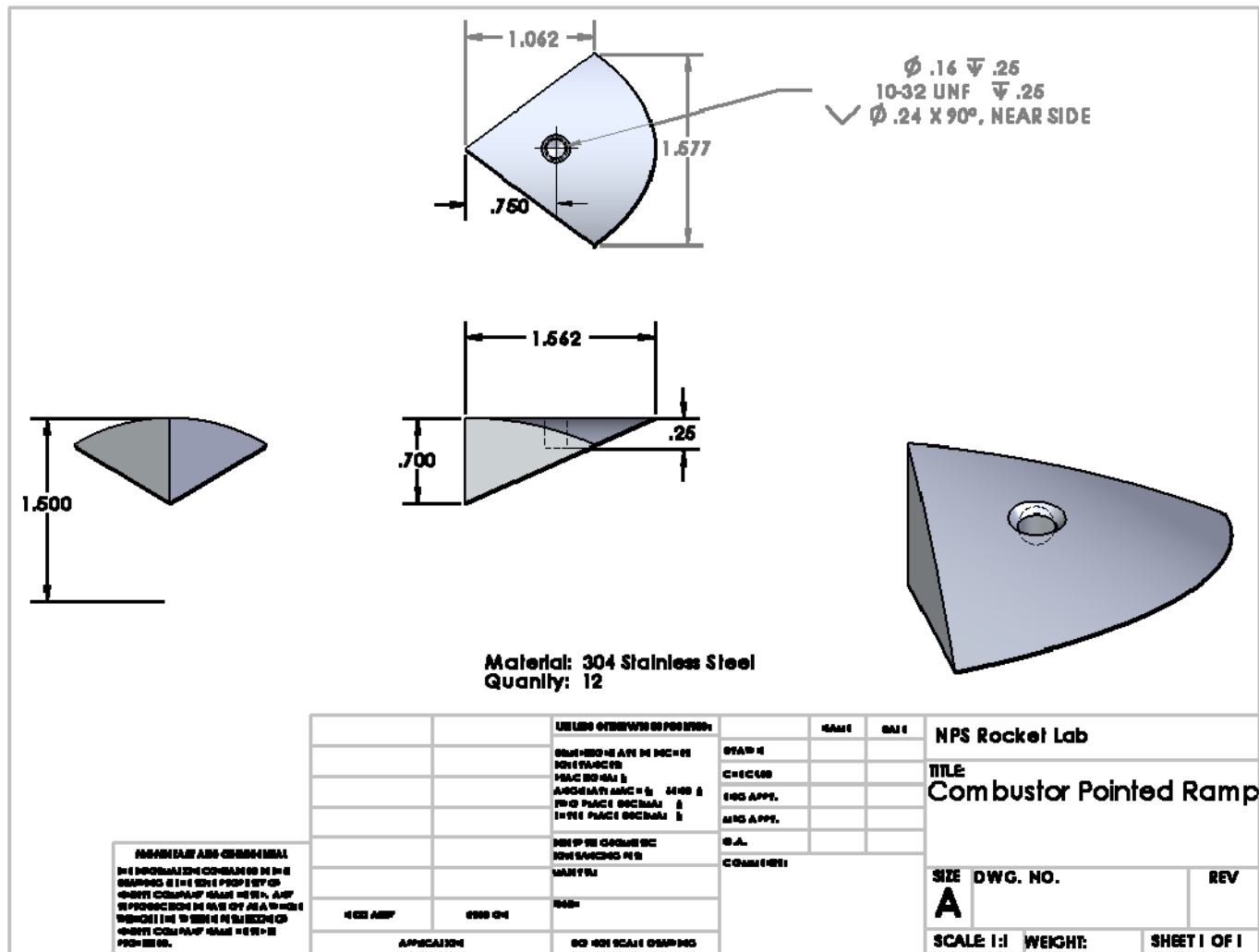
Figure 51.    Pointed ramp

71

THIS PAGE INTENTIONALLY LEFT BLANK

# APPENDIX D:  LEGENDS FOR PRESSURE LOSS CURVES

| | |
|---|---|
| ———— | 1R.360.6S.cold.nonoz.final.09Jul09pr09.DP.P3.LM.Re.txt |
| ———— | 1R.360.8S.cold.nonoz.final.08Jul09pr05.DP.P3.LM.Re.txt |
| ———— | 1R.360.8S.cold.nonoz.final.23Jul09pr01.DP.P3.LM.Re.txt |
| ———— | 1R.360.8S.cold.nonoz.final.unswept.29Jul09pr02.DP.P3.LM.Re.txt |
| ———— | 2R.180.4S.cold.nonoz.final.19Aug09pr04.DP.P3.LM.Re.txt |
| ———— | 2R.180.4S.cold.nonoz.final.interdig.31Jul09pr01.DP.P3.LM.Re.txt |
| ———— | 2R.180.4S.cold.nonoz.final.nonswept.13Jul09pr01.DP.P3.LM.Re.txt |
| — — | 2R.180.5S.cold.nonoz.final.19Aug09pr01.DP.P3.LM.Re.txt |
| — — | 2R.180.5S.cold.nonoz.final.interdig.29Jul09pr10.Dp.P3.LM.Re.txt |
| — — | 2R.180.5S.cold.nonoz.final.pointed.31Jul09pr02.DP.P3.LM.Re.txt |
| — — | 2R.180.5S.cold.nonoz.final.short.20Aug09pr01.DP.P3.LM.Re.txt |
| — — | 2R.180.6S.cold.nonoz.final.30Jul09pr01.DP.P3.LM.Re.txt |
| — — | 2R.180.6S.cold.nonoz.final.unswept.29Jul09pr05.DP.P3.LM.Re.txt |
| — — | 2R.180.8S.cold.nonoz.final.22Sep09pr09.DP.P3.LM.Re.txt |
| —·—·— | 2R.180.8S.cold.nonoz.final.pointed.31Jul09pr03.DP.P3.LM.Re.txt |
| —·—·— | 3R.120.4S.cold.nonoz.final.10Jul09pr04.DP.P3.LM.Re.txt |
| —·—·— | 3R.120.6S.cold.nonoz.final.10Jul09pr01.DP.P3.LM.Re.txt |
| —·—·— | 4R.090.4S.cold.nonoz.final.08Jul09pr03.DP.P3.LM.Re.txt |
| —·—·— | ramp.spiral.4S.cold.nonoz.final.13Jul09pr05.DP.P3.LM.Re.txt |
| —·—·— | ramp.spiral.8S.cold.nonoz.final.13Jul09pr04.DP.P3.LM.Re.txt |
| —·—·— | sch.spiral.cold.nonoz.final.18Aug09pr01.DP.P3.LM.Re.txt |
| —··—··— | 2R.180.4S.cold.nonoz.final.unsweptwide.09Nov09pr07.DP.P3.LM.Re.txt |
| —··—··— | 2R.180.5S.cold.nonoz.final.unsweptwide.09Nov09pr06.DP.P3.LM.Re.txt |
| —··—··— | 2R.180.6S.cold.nonoz.final.unsweptwide.09Nov09pr03.DP.P3.LM.Re.txt |

Table 6.      Legend for Figure 25

| | |
|---|---|
| ———— | 1R.360.6S.cold.nonoz.final.09Jul09pr09.DP.P3.LM.Re.txt |
| ———— | 1R.360.8S.cold.nonoz.final.08Jul09pr05.DP.P3.LM.Re.txt |
| ———— | 1R.360.8S.cold.nonoz.final.23Jul09pr01.DP.P3.LM.Re.txt |
| ———— | 1R.360.8S.cold.nonoz.final.unswept.29Jul09pr02.DP.P3.LM.Re.txt |
| ———— | 2R.180.4S.cold.nonoz.final.19Aug09pr04.DP.P3.LM.Re.txt |
| ———— | 2R.180.4S.cold.nonoz.final.interdig.31Jul09pr01.DP.P3.LM.Re.txt |
| ———— | 2R.180.4S.cold.nonoz.final.nonswept.13Jul09pr01.DP.P3.LM.Re.txt |
| — — | 2R.180.5S.cold.nonoz.final.19Aug09pr01.DP.P3.LM.Re.txt |
| — — | 2R.180.5S.cold.nonoz.final.interdig.29Jul09pr10.Dp.P3.LM.Re.txt |
| — — | 2R.180.5S.cold.nonoz.final.pointed.31Jul09pr02.DP.P3.LM.Re.txt |
| — — | 2R.180.5S.cold.nonoz.final.short.20Aug09pr01.DP.P3.LM.Re.txt |
| — — | 2R.180.6S.cold.nonoz.final.30Jul09pr01.DP.P3.LM.Re.txt |
| — — | 2R.180.6S.cold.nonoz.final.unswept.29Jul09pr05.DP.P3.LM.Re.txt |
| — — | 2R.180.8S.cold.nonoz.final.22Sep09pr09.DP.P3.LM.Re.txt |
| ·········· | 2R.180.8S.cold.nonoz.final.pointed.31Jul09pr03.DP.P3.LM.Re.txt |
| ·········· | 3R.120.4S.cold.nonoz.final.10Jul09pr04.DP.P3.LM.Re.txt |
| ·········· | 3R.120.6S.cold.nonoz.final.10Jul09pr01.DP.P3.LM.Re.txt |
| ·········· | 4R.090.4S.cold.nonoz.final.08Jul09pr03.DP.P3.LM.Re.txt |
| ·········· | ramp.spiral.4S.cold.nonoz.final.13Jul09pr05.DP.P3.LM.Re.txt |
| ·········· | ramp.spiral.8S.cold.nonoz.final.13Jul09pr04.DP.P3.LM.Re.txt |
| ·········· | sch.spiral.cold.nonoz.final.18Aug09pr01.DP.P3.LM.Re.txt |

Table 7.      Legend for Figure 27

□     1R.360.6S.cold.smnoz.final.09Jul09pr07.DP.P3.LM.Re.txt
□     1R.360.8S.cold.smnoz.final.08Jul09pr06.DP.P3.LM.Re.txt
□     2R.180.4S.cold.smnoz.final.19Aug09pr03.DP.P3.LM.Re.txt
□     2R.180.4S.cold.smnoz.final.nonswept.13Jul09pr02.DP.P3.LM.Re.txt
□     2R.180.5S.cold.smnoz.final.19Aug09pr02.DP.P3.LM.Re.txt
□     2R.180.5S.cold.smnoz.final.interdig.29Jul09pr11.DP.P3.LM.Re.txt
△     2R.180.5S.cold.smnoz.final.short.20Aug09pr02.DP.P3.LM.Re.txt
△     2R.180.6S.cold.smnoz.final.22Sep09pr07.DP.P3.LM.Re.txt
△     2R.180.8S.cold.smnoz.final.22Sep09pr08.DP.P3.LM.Re.txt
△     3R.120.4S.cold.smnoz.final.10Jul09pr03.DP.P3.LM.Re.txt
△     3R.120.6S.cold.smnoz.final.10Jul09pr02.DP.P3.LM.Re.txt
△     4R.090.4S.cold.smnoz.final.08Jul09pr04.DP.P3.LM.Re.txt
◇     ramp.spiral.4S.cold.smnoz.final.13Jul09pr06.DP.P3.LM.Re.txt
◇     ramp.spiral.8S.cold.smnoz.final.13Jul09pr03.DP.P3.LM.Re.txt
◇     sch.spiral.cold.smnoz.final.18Aug09pr02.DP.P3.LM.Re.txt
◇     2R.180.4S.cold.smnoz.final.unsweptwide.09Nov09pr08.DP.P3.LM.Re.txt
◇     2R.180.5S.cold.smnoz.final.unsweptwide.09Nov09pr05.DP.P3.LM.Re.txt
◇     2R.180.6S.cold.smnoz.final.unsweptwide.09Nov09pr04.DP.P3.LM.Re.txt

Table 8.     Legend for Figure 29

———— 1R.360.6S.cold.smnoz.final.09Jul09pr07.DP.P3.LM.Re.txt
———— 1R.360.8S.cold.smnoz.final.08Jul09pr06.DP.P3.LM.Re.txt
———— 2R.180.4S.cold.smnoz.final.19Aug09pr03.DP.P3.LM.Re.txt
———— 2R.180.4S.cold.smnoz.final.nonswept.13Jul09pr02.DP.P3.LM.Re.txt
———— 2R.180.5S.cold.smnoz.final.19Aug09pr02.DP.P3.LM.Re.txt
———— 2R.180.5S.cold.smnoz.final.interdig.29Jul09pr11.DP.P3.LM.Re.txt
— — 2R.180.5S.cold.smnoz.final.short.20Aug09pr02.DP.P3.LM.Re.txt
— — 2R.180.6S.cold.smnoz.final.22Sep09pr07.DP.P3.LM.Re.txt
— — 2R.180.8S.cold.smnoz.final.22Sep09pr08.DP.P3.LM.Re.txt
— — 3R.120.4S.cold.smnoz.final.10Jul09pr03.DP.P3.LM.Re.txt
— — 3R.120.6S.cold.smnoz.final.10Jul09pr02.DP.P3.LM.Re.txt
— — 4R.090.4S.cold.smnoz.final.08Jul09pr04.DP.P3.LM.Re.txt
·············· ramp.spiral.4S.cold.smnoz.final.13Jul09pr06.DP.P3.LM.Re.txt
·············· ramp.spiral.8S.cold.smnoz.final.13Jul09pr03.DP.P3.LM.Re.txt
·············· sch.spiral.cold.smnoz.final.18Aug09pr02.DP.P3.LM.Re.txt

Table 9.     Legend for Figure 30

# LIST OF REFERENCES

[1]     K. K. Kuo, *Principles of Combustion*. New Jersey: John Wiley & Sons, Inc., 1986.

[2]     K. Kailasanath, "Recent developments in the research on pulse detonation engines," *AIAA Journal*, vol. 41, pp. 145–159, February 2003.

[3]     H. Hoffmann, "Reaction-propulsion produced by intermittent detonative combustion," *German Research Institute for Gliding*, ATI-52365, August 1940.

[4]     J. A. Nicholls, H. R. Wilkinson, and R. B. Morrison, "Intermittent detonation as a thrust-producing mechanism," *Jet Propulsion*, pp. 534–541, May 1957.

[5]     L. J. Krzycki, "Performance characteristics on an intermittent-detonation device", report 7655, AD-284312, *U.S. Naval Ordnance Test Station NAVWEPS*, June 1962.

[6]     D. Helman, R. P. Shreeve, and S. Eidelman, "Detonation pulse engine," AIAA paper 1986-1683, *22$^{nd}$ AIAA/ASME/SAE/ASEE Joint Propulsion Conference*, June 1986.

[7]     T. Bussing and G. Pappas, "An introduction to pulse detonation engines," AIAA Paper 1994-0263, *32$^{nd}$ AIAA Aerospace Sciences Meeting and Exhibit*, Reno, Nevada, January 1994.

[8]     G. D. Roy, "Status of Navy PDE research," PowerPoint presentation, *Office of Naval Research PDE Workshop*, Dayton, Ohio, 12 September 2002.

[9]     S. I. Jackson and J. E. Shepherd, "Initiation systems for pulse detonation engines," *38$^{th}$ AIAA/ASME/SAE/ ASEE Joint Propulsion Conference and Exhibit*, July 2002, Indianapolis IN, AIAA 2002-2627, 2002.

[10]    J. O. Sinibaldi, C. M. Brophy, C. Li, and K. Kailasanath, "Initiator detonation diffraction studies in pulse detonation engines," AIAA-2001-3466, 37th *AIAA/ASME/SAE/ASEE Joint Propulsion Conference and Exhibit*, Salt Lake City, UT, July 2001.

[11]    C. M. Brophy, S. Werner, and J. O. Sinibaldi, "Performance characterization of a valveless pulse detonation engine," AIAA paper 2003-1344, *41$^{st}$ AIAA Aerospace Sciences Meeting and Exhibit*, Reno, Nevada, January 2003.

[12]    S. Y. Lee, J. Watts, S. Saretto, S. Pal, C. Conrad, R. Woodward, and R. Santoro, "Deflagration to detonation transition processes by turbulence-generating obstacles in pulse detonation engines," Journal of Propulsion and Power, vol. 20 no. 6, 2004, pp. 1026–1036.

[13]    J. O. Sinibaldi, C. M. Brophy, and LT J. P. Robinson, "Ignition effects on deflagration-to-detonation transition distance in gaseous mixtures", AIAA2000-3590, *36th AIAA/ASME/SAE/ASEE Joint Propulsion Conference*, Huntsville, AL. July 2000.

[14]    F. Schauer, J. Stutrud, and R. Bradley,"Detonation initiation studies and performance results for pulsed detonation engine applications," *AIAA-2001-1129, Aerospace Sciences Meeting and Exhibit*, 39th, Reno, Nevada, January 2001

[15]    P. D. Hutcheson, C. M. Brophy, and J. O. Sinibaldi "Investigation of flow field properties on detonation initiation" AIAA Paper 2006-5099, *Joint Propulsion Conference and Exhibit,* Sacramento, California, July 2006.

[16]    M. Cooper, S. Jackson, J. Austin, E. Wintenberger, J. E. Shepherd, "Direct experimental impulse measurements for detonations and deflagrations," *Journal of Propulsion and Power 2002*, 0748-4658, vol. 18, no. 5, pp. 1033–1041.

[17]     D. Paxson, F. Schauer, "Performance impact of deflagration to detonation transition enhancing obstacles"  AIAA-2009-502, *47th AIAA Aerospace Sciences Meeting*, Orlando, Florida, January 2009.

[18]    R. P. Lindstedt and H. J. Michels, "Deflagration to detonation transitions and strong deflagrations in alkane and alkene mixtures with O2/N2," *Combustion and Flame*, vol. 76, pp. 169–189, 1989.

[19]    T. S. Kuan, R. P. Lindstedt and E. M. Vaos, "Higher moment based modeling of turbulence enhanced explosion kernels in confined fuel-air mixtures," Confined Detonations and Pulsed Detonation Engines, edited by G.D. Roy, S.M. Frolov, R.J. Santoro, and S.A. Tsyganov, Torus Press, Moscow, Russia, 2003, pp. 17–40.

[20]    A. J. Higgins, P. Pinard, A. C. Yoshinaka, and J. H. S. Lee, "Sensitization of fuel-air mixtures for deflagration-to-detonation transition," in G. Roy, S. Frolov, D. Netzer, and A. Borisov, Eds., *High-Speed Deflagration and Detonation: Fundamentals and Control*, pp. 45–49, ELEX-KM Publishers, 2001.

[21]    P. D. Hutcheson, "Design, modeling and performance of a Split path JP-10/Air Pulse Detonation Engine," M.S. thesis, Naval Postgraduate School, Monterey, CA, December 2006.

[22]    N. C. Hawkes, "Characterization of transient plasma ignition kernel growth for varying inlet condition," M.S. thesis, Naval Postgraduate School, Monterey, CA, December 2009.

[23]    Operations and Maintenance Manual, *Six Component, 500 Pound Pulse Detonation Measurement System,* Pacific Press Co., N00244-02-C-0060, Manual No. 110028, September 2002.

[24]    B. J. Bartosh, "Thrust measurement of a split-path valveless pulse detonation engine,"  M.S. thesis, Naval Postgraduate School, Monterey, CA, December 2007.

THIS PAGE INTENTIONALLY LEFT BLANK

# INITIAL DISTRIBUTION LIST

1.      Defense Technical Information Center
        Ft. Belvoir, Virginia

2.      Dudley Knox Library
        Naval Postgraduate School
        Monterey, California

3.      Prof. Chris Brophy
        Naval Postgraduate School
        Monterey, California

4.      Dr. Anthony Gannon
        Naval Postgraduate School
        Monterey, California

5.      LT William Dvorak
        Naval Postgraduate School
        Monterey, California